Paper Preprints

RTN'2011

10th International Workshop on Real-Time Networks

Porto, Portugal, July 5th 2011

In conjunction with:

23rd Euromicro International Conference on Real-Time Systems

Porto, Portugal, July 6th - 8th 2011

Editor: Michael Short
Electronics & Control Group, Teesside University, UK.

10th International Workshop on Real-Time Networks

Paper Preprints

Contents

Editor: Michael Short

Message from the Chair

Welcome to Porto!

It has been a pleasure to be involved with the organisation and preparation for this year's international workshop on real-time networks, the 10th in a series which initially started as the RTLIA workshop at the 2002 ECRTS conference in Vienna.

This year the workshop received 15 submissions, each of which was reviewed by at least three members of the program committee. Out of the 15 submissions, seven papers were very carefully selected for presentation at the workshop and to be included in the final proceedings, to be published in December 2011. In addition, the workshop also features a keynote speech, an industry lecture and a panel discussion session.

Our aim is to closely follow previous years with an interactive format and plenty of time allocated for discussion during each of the sessions. Thanks must go to the authors and presenters for their hard work, and also to the committee members for their thoughtful and in-depth reviews. Everyone involved has contributed significantly to what promises to be a thought provoking and interesting day.

Thanks are also due to all who have assisted the organisation process, including the ECRTS and RTN committee members and the CISTER-ISEP members who have helped with local arrangements. Especially worthy of praise are Gerhard Fohler, Karl-Erik Årzén, Stefan Petters, Jean-Dominique Decotignie and Luis Almeida. Finally, thanks must also go to Eduardo Tovar, and to echo his words as the 1st program chair almost a decade ago, I sincerley hope that there are many future RTN workshops!

I hope that you will find this year's workshop informative and, above all, enjoyable.

Michael Short

Middlesbrough, Teesside, UK.

International Program Comittee

Luis Almeida (University of Porto, Portugal)

Leandro Buss Becker (Federal University of Santa Catarina, Brazil)

Gianluca Cena (Politecnico di Torino, Italy)

Jean-Dominique Decotignie (Swiss Center for Microtechnology CSEM)

Zdenek Hanzalek (TU Prague, Czech Republic)

Sheikh Imran (University of Leicester, UK)

Anis Koubaa (Al-Imam University, KSA & CISTER Research Unit, Portugal)

Lucia Lo Bello (University of Catania, Italy)

Pau Marti (Technical University of Catalonia, Spain)

Daniel Mosse (University of Pittsburgh, USA)

Luca Mottola (SICS, Sweden)

Binoy Ravindran (Virginia Tech, USA)

Michael Schwarz (Universitat Kassel, Germany)

Michael Short (Teesside University, UK).

Ye-Qiong Song (LORIA, France)

Eduardo Tovar (IPP-HURRAY, Portugal)

Andreas Willig (University of Canterbury, New Zealand)

Workshop Program

Registration (08:30-09:00)

Welcome (09:00-09:10)

Session 1: Mobility in Real-Time Networks
Chair: Zdeněk Hanzálek

Paper 1 (09:10-09:50) On the Use of Code Mobility Mechanisms in Real-time Systems
Luís Lino Ferreira and Luís Nogueira (Polytechnic Institute of Porto, Portugal)

Paper 2 (09:50-10:30) Evaluating the Benefits and Feasibility of Coordinated Medium Access in MANETS
Authors: Marcelo Maia Sobral and Leandro Buss Becker (Federal University of Santa Catarina, Brazil)

Coffee Break (10:30-10:50)

Session 2: Automotive Networks
Chair: Michael Short

Paper 3 (10:50-11:30) Time Constrained FlexRay Static Segment Scheduling
Authors: Zdeněk Hanzálek, David Benes and Denis Waraus (Czech Technical University in Prague, Czech Republic)

Keynote Speech (11:30-12:30) The case for Ethernet in Automotive Communications
Speaker: Lucia Lo Bello (University of Catania, Italy)

Lunch Break (12:30-13:30)

Session 3: Wireless Sensor Networks and Applications
Chair: Mário Alves

Paper 4 (13:30-14:10) The Possibility of Wireless Sensor Networks for Commercial Vehicle Load Monitoring
Authors: Jieun Jung, Byunghun Song and Sooyeol Park (RFID/USN Convergence Centre, Republic of Korea / IT Convergence Research Center, Republic of Korea)

Paper 5 (14:10-14:50) Real-time routing for low-latency 802.15.4 control networks
Authors: Koen Holtman and Peter van der Stok (Philips Research, Eindhoven, The Netherlands).

Paper 6 (14:50-15:30) Quantifying the Channel Quality for Interference-Aware Wireless Sensor Networks
Authors: Claro Noda, Shashi Prabh, Carlo Alberto Boano, Thiemo Voigt and Mário Alves (Polytechnic Institute of Porto, Portugal / Universitat zu Lubeck, Germany / Swedish Institute of Computer Science, Kista, Sweden)

Workshop Program (cont.)

Coffee Break (15:30-15:50)

Session 4: Avionic Networks
Chair: Eduardo Tovar

Paper 7 (15:50-16:30) Existing offset assignments are near optimal for an industrial AFDX network
Authors: Xiaoting Li, Jean-Luc Scharbarg, Christian Fraboul and Frédéric Ridouard (Université de Toulouse, France / University of Poitiers, France).

Industry Lecture (16:30-17:30) Networking in Modern Avionics: Challenges and Opportunities
Speaker: Sérgio Duarte Penna (Embraer S.A., São José dos Campos, Brazil).

Session 5: Future Directions in Real-Time Network Research
Chair: Jean-Dominique Decotignie (CSEM, Switzerland)

Panel Discussion (17:30-Close)
Sérgio Duarte Penna (Embraer S.A., Brazil)
Lucia Lo Bello (University of Catania, Italy)
Christian Fraboule (Université de Toulouse, France)
Hermann Kopetz (Vienna University of Technology, Austria)

Keynote speech: The case for Ethernet in Automotive Communications

Lucia Lo Bello
Department of Electric, Electronic and Computer Engineering
University of Catania, Italy
{lucia.lobello@dieei.unict.it}

Abstract

The spreading of Ethernet as an in-vehicle network for today's cars or those in the near future is being broadly announced by spokespersons for major carmakers and automotive electronics companies. Even in the scientific community there is a growing interest in the topic, as is shown by the increasing number of studies that address the performance of Switched Ethernet or Time-Triggered Ethernet in automotive embedded systems. Several factors seem to favour the introduction of Ethernet technology in the automotive communication systems arena. Some of them are similar to those that, ten years ago, motivated the interest towards the introduction of Ethernet in automation as either a complement or replacement of traditional fieldbuses. The main motivation is the higher bandwidth provided by Ethernet (100 Mbps) as compared to current in-car networks. Such an increased bandwidth paves the way for applications, like advanced driver assistance systems, which make the volume of exchanged data in automotive communication continuously grow. Other enabling factors for using Ethernet as automotive communication network are the assessed technology and the support offered to the Internet Protocol stack (IP). The Diagnostics over Internet Protocol (DoIP) standard, currently under specification as ISO 13400, will foster the use of Ethernet as a replacement for CAN for the reprogramming (flashupdate) and in-car diagnostics of automotive Electronic Control Units (ECUs). With Internet connectivity, the IP protocol will be used in-car, opening the way to enhanced navigation functionalities, remote diagnostics and location-based services. In addition to the above mentioned features, Ethernet technology is scalable, thus meeting the scalability requirement imposed by today's automotive systems, where the number of nodes to interconnect steadily increases. The automotive domain is however quite different from automation environments. An in-car embedded system is typically divided into several functional domains, that feature different requirements and specific constraints.In this context, the talk will discuss how and to what extent Ethernet technology is likely to step in and provide benefits to the different automotive functional domains. The potential for making Ethernet a complement or even replacement to other network technologies in their respective functional domain will be addressed. The talk will consider the TTEthernet protocol, as its design provides several appealing features for automotive communication, such as, determinism, fault-tolerance, independence of fault-containment regions, fault-tolerant global time, and legacy Ethernet integration. Recent works, in fact, addressed performance evaluation of TTEthernet. The talk will both summarise significant results from related works and present new performance results obtained in some selected case studies. Finally, some directions for further investigation into the adoption of Ethernet in cars will be given, with some reference to running projects.

Speaker Biography

Lucia Lo Bello is Associate Professor with tenure in the Department of Computer Engineering and Telecommunications at the University of Catania. Her research interests include wireless networks and sensor networks, factory communication, distributed process control, real-time industrial embedded systems, energy-aware protocols. She received the M.D. in Electronic Engineering in 1994 and the PhD degree in Computer Engineering in 1998, both from the University of Catania. She was a visiting researcher at the Department of Computer Engineering of Seoul National University, South Korea (2000-01) with a post-doctoral position. She has served on a number of program committees of distinguished international conferences in the area of factory communication, industrial embedded systems and real-time systems, being also General Chair and Program Co-Chair of some of them. She is reviewer for several international journals. She is responsible for the University of Catania of the flexWARE Project, Flexible Wireless Automation in Real-Time Environments and the ARTISTDesign NoE on Embedded Systems Design, both projects funded by the European Commission within the 7 FP. Member of the IEC Subcommittee 65C, she actively partecipates to the standardization process. She is the recipient of the IEEE Industrial Electronics Society 2008 Early Career Award. Since 2009, she is Senior Member of the IEEE. She has published more than 120 technical papers on international conferences, books and journals in the area of wireless sensor networks, factory communication, real-time systems and distributed systems.

Industry Lecture: Networking in Modern Avionics - Challenges and Opportunities

Sérgio Duarte Penna

Embraer S.A., São José dos Campos, Brazil)
{sdpenna@embraer.com.br}

Abstract

The introduction of "Integrated Modular Avionics" (IMA) by the Radio Technical Commission for Aeronautics (RTCA DO-297) in November 2005 gave focus to new industry standards. "Avionics Full Duplex Switched Network" (ARInc 644 Part 7 "AFDX"), "Time-Triggered Protocol" (TTA Group "TTP") and "Application Executive interface" (ARInc 653 "APEX") emerged offering new levels of modularity and communality to avionic systems. These standards present new challenges for system manufacturers and integrators, but offer new opportunities to improve current analytical methods for predicting system behaviour during the design phase. This presentation provides a quick overview of these important standards and addresses challenges and opportunities arising from their adoption.

Speaker Biography

Sérgio Penna graduated as a Mechanical Engineer in 1978 by the Federal University of Minas Gerais in Belo Horizonte, Brazil. He joined EMBRAER in 1982 as a computer analyst working for the Flight Test Division where he is still on duty. In 2008, he obtained his Master's Degree at the National Institute of Space Research (INPE) in São José dos Campos, Brazil, in Space Engineering and Technology. He is currently responsible for a team of 5 people working at EMBRAER's Flight Test Ground Station in charge of in-house software development for flight test data post-processing systems.

On the Use of Code Mobility Mechanisms in Real-time Systems

Luís Lino Ferreira, Luís Nogueira
{llf, lmn}@isep.ipp.pt
CISTER/ISEP - Polytechnic Institute of Porto
Porto, Portugal

Abstract - **Applications with soft real-time requirements can benefit from code mobility mechanisms, as long as those mechanisms support the applications' timing and Quality of Service requirements. In this paper, a generic model for code mobility mechanisms is presented. The proposed model gives system designers the necessary tools to perform a statistical timing analysis on the execution of the mobility mechanisms that can be used to determine the impact of code mobility in distributed real-time applications.**

Index Terms—**Real-time systems, distributed embedded systems, mobile systems, code mobility, quality of service**

I. Introduction

Open real-time systems are increasingly shifting from a set of small, local applications to powerful resource-hungry distributed applications [4]. By the very nature of open real-time systems, the availability of resources is unknown before hand and can only be reserved dynamically as new applications arrive to the system. Consequently, there is an increasing demand for supporting distributed applications with the flexibility to offload parts of their computations to neighbour or "in the cloud" nodes due to local resource scarcity. Nevertheless, the real-time behaviour of these applications must be guaranteed, both during execution and during reconfiguration, after mobility has occurred.

Therefore, open real-time systems must provide applications the support to: i) use services provided by remote components; ii) move part(s) of the application's code to remote nodes; and ii) guarantee real-time behaviour. The first requirement can be supported by a service-based infrastructure [4], to easily and transparently interconnect local and remote parts of an application. The second requirement can be supported by code mobility frameworks which allow the installation and execution of parts of an application in remote nodes [9]. Finally, the third requirement can be supported by a real-time resource manager. Capacity reserves have been proved to be successful in improving the response times of soft real-time tasks while preserving all hard real-time constraints, both CPU [3] and network [2].

A. Related work

Although not widely studied, a few solutions have already been proposed to analyse the impact of code mobility on the real-time requirements of applications.

In [11], the authors propose and experimentally characterise the behaviour of a hard real-time framework that supports the migration of tasks between nodes. However, the work does not propose a mathematical model that enables system designers to account for the impact of the mobility protocol on the overall timing behaviour of applications.

A strategy for minimising the impact of code mobility in a hierarchical preemptive fixed priority scheduling system for Real-Time Java is proposed in [10]. The authors mainly determine the points in time at which the migration process should be started, which guarantees that tasks' deadlines are met and that the migration process is executed between consecutive evocations of a migratable task.

Statefull services require the transfer of state, whose duration depends on the length of the data being transferred. However, during this period of time no transactions can be executed on that service (blackout time). However, such determination is only possible in systems with a well-known and controlled timing behaviour. Therefore, in [12], the authors tackled the problem of minimising the blackout time by proposing a partial blocking and a non-blocking approach for state transfer.

Nevertheless, none of these works focus on the mobility mechanism itself. A mobility framework should also enable the runtime relocation of services in response to reconfiguration/update events (*e.g.*, the system might reconfigure itself due to the disappearance of a node involved in a computation). As an example, consider running a video game on a mobile device that offloads parts of its computations to neighbour nodes. Reconfiguration in such a cooperative execution might be required if one of the nodes, currently running one of game's services, is no longer capable of outputting the required QoS. In such case, the service should be migrated to another node. Ideally, such change should be executed seamlessly, i.e. the game delays should (preferably) be unnoticeable. Examples of works that tackle

the specific problems stated above are [4] and [1]. The former allows the determination of a distributed configuration that maximises the satisfaction of the user's QoS preferences among a set of allowed QoS levels. The latter tries to fulfil the same goals, but each service is only allowed to specify a single QoS level.

B. Contribution and paper structure

Service mobility in a distributed execution environment is a complex operation that evolves through several phases, including sending the code and state to the destination node and rebinding connections between services. Additionally, resources must be explicitly reserved on the destination node, prior to the start of the mobility process. Due to its complexity, we propose that a Mobility Management framework (represented in Figure 1 by M_x) should control mobility of services between nodes of a distributed system. This paper focuses on the model and timing analysis for a generic code mobility mechanism for distributed soft real-time applications. The proposed model is generic enough, helping the system designer to define the most appropriate parameters for the mobility management modules and to determine the feasibility of the timing constrains imposed on applications, including mobility/reconfiguration events.

The remainder of the paper is organised as follows. Section II defines the generic model for the distributed applications and for the mobility mechanism. Section III discusses and analyses the code mobility phases and their timings. The main consequence of the mobility mechanism is the introduction of a bounded inaccessibility period during which the service being moved is not available. The proposed analysis allows computing the adequate resources required by the mobility framework to guarantee the timeliness of the application. Finally, Section IV discusses the model provided in the paper and presents some conclusions.

II. System Model

A. Module components

This work applies to soft real-time applications composed by a set of interconnected services, each supplying some service, either in the same local node, but particularly when services are distributed among several nodes. The model considers the system to be composed of a set of N nodes $\{H_1, ..., H_N\}$ and a set of M services $\{S_1, \ldots, S_M\}$. Services are interconnected through links. $l_{x,y}$ characterises a connection between services S_x and S_y, (Figure 1). Each service and each link has a set of real-time requirements that are out of the scope of this paper (a detailed discussion can be found in [4]).

Each node runs a *Mobility Management* module M_x, where x is the index of the node. Each module M_x can be connected to other Mobility Management modules M_y through a network connection, $l_{mx,my}$.

As depicted in Figure 1, an operation $m^{S5}{}_{H3\rightarrow H4}$ represents the mobility of service S_5 between nodes H_3 and H_4. In such case, H_3 is denoted as the *source* node and H_4 is denoted as the *destination* node. Link $l'_{6,5}$ represents the connection that has to be established after the mobility operation is completed (rebinding). Consequently, connection $l_{6,5}$ will have to be safely deleted prior to $l'_{6,5}$ becomes operational. By safely, we mean that no messages should be lost or delivered to wrong nodes. This operation implies offloading the code of S_5, its data state, and rebinding its connections, all within timing constraints.

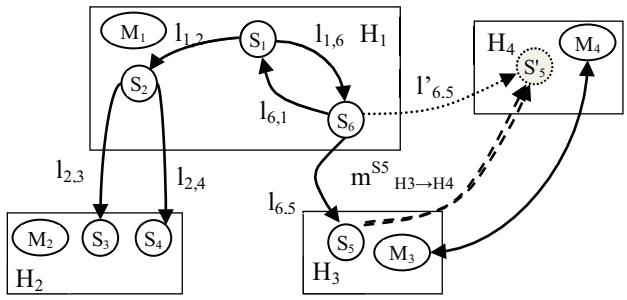

Figure 1 – System Model

B. Resource management

It is assumed that access to the system's resources can be modelled as a set of isolated servers, either related to the CPU [3] or network [2] scheduling. Each of these servers is characterised by its maximum reserved capacity (Q_i) that can be used during a period (T_i); at the end of this period the capacity is replenished. Other CPU schedulers can also be used, like the Capacity Sharing and Stealing scheduler (CSS) proposed in [13]. For the network scheduling, any scheduling algorithm with similar characteristics can also be used, like the ones based on the Flexible Time-Triggered approach [14].

Based on these guarantees, it is possible to determine services' average response time using the formulations proposed in [3]:

$$R_i^{avg} = C_i^{avg} + (T_i - Q_i) \sum_{k=0}^{+\infty} \left(1 - F_C(k \times Q_i)\right) \quad (1)$$

where $C^{avg}{}_i$ represents the average execution time of task T and $F_C(x)$ is the cumulative distribution function (c.d.f.) of the task's execution time. In the remainder of the paper, we will use the notation $R(Q_i, T_i, F_C^i())$ to represent Equation (1).

C. Mobility Management Framework

We assume the existence of a modular Mobility Management framework in each node, similar to the one proposed in [9].

These mobility management modules have CPU and networking servers assigned to them, guaranteeing the timing requirements of its operations. Servers associated with the CPU offer a capacity of C_F over a period T_F. Network resources are split between two channels, one for bulky data

transfer and another for the exchange of short control messages. The first has a capacity of B_{data} and a period of T_{data} while the second has a capacity of B_{ctrl} and a period of T_{ctrl}. The main advantage of using these two channels is that we can guarantee small response time for control messages, but for larger data transfer we are able to make the transfer with small overhead.

D.Service's internal state

In the proposed model, services are able to split their internal state into different *State Items*, representing different variables, different objects or combinations of both. It is up to the service to define how state items are configured. The state of a service is thus a set of state items defined exclusively by the service, where a State Item (SI^{Si}_{p}) is only associated to a service S_i and defined as a tuple:

$$SI_p^{Si} = \left\{ID_p^{Si}, B_p^{Si}\right\}$$

ID^{Si}_{p} univocally identifies this State Item and B^{Si}_{p} is the bandwidth required for the transfer of this state item. Some state items are created during the service initialisation and are not changed subsequently, while others are updated regularly when service calls are executed. Therefore, state items are divided in two groups: one that can be migrated during the normal operation of the service (S*tatic Sate Items*) and another that can only be migrated if there are no ongoing service calls (*Dynamic State Items*).

Based on the model exposed in this section, Section III shows how it is possible to devise a timing model for a generic mobility mechanism.

III. CODE MOBILITY TIMING MODEL

Service mobility can be split in two main phases: *Preparatory* and *Blackout* phases. During the *Preparatory* phase, the migrating service continues operational in the source node. This phase is further divided into three subphases: *mobility decision*, *code shipping*, and *initial state transfer*. During the *Blackout* phase, the service is totally inaccessible to others. It includes the subphases: *state transfer*, *connections rebinding*, and *service restart*. Some of the subphases are executed serially while others can be executed in parallel. Figure 2 depicts a timeline containing an example of a mobility procedure. A detailed description and analysis of each step is given in the following subsections. In this analysis, for the sake of simplicity, we assume that no other service mobility operation occurs during the complete procedure and that a higher-level resource control framework assures such control.

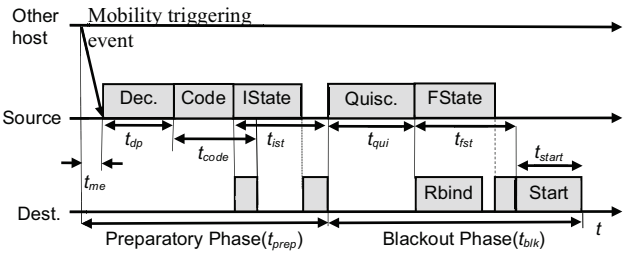

Figure 2 – Mobility-related timings

A. Preparatory Phase

1) Decision process

The start of service mobility (*mobility triggering event*) results from a decision by the application (currently using the service) or by request from an external entity (the user, another application or specific framework). As an example, in Figure 2, the triggering event is received from another node.

State changes can also trigger service mobility whenever a user requests the execution of an application that can only be admitted into the system if the system is reconfigured by migrating some services of previously admitted applications to neighbour nodes. As an example, consider that a user decides to play an mp3 file in its mobile device, having to migrate part of a local application to a neighbour notebook.

Note that migration can only be allowed if there is a feasible system configuration that allows the service to continue operating within its required QoS levels. Algorithms such as those provided by the Prism [1] or CooperatES [4] frameworks take a high-level approach, finding a solution for the distribution of the application services between nodes in a way that maximises a global utility function and, simultaneously, guarantees enough resources (CPU, network, memory, etc) for every admitted service. While the former assumes just one possible QoS level to the application, the latter assumes that each service can work with multiple QoS levels, each one with a different utility value to the overall system. Additionally, the algorithms proposed in [4] are capable of generating a system configuration in a bounded amount of time. These algorithms are able to use a global view of the system state or can simply use a partial view of the system, e.g. if the node computing a decision only has access to a limited number of nodes.

We should point out that the algorithms proposed in [1] and [2] do not take into account the cost introduced by systems reconfiguration and particularly code mobility.

2) Code shipping

After finding a new distributed solution, the source node informs the destination node of the QoS requirements for the service being migrated. The destination node can then make all necessary local confirmations on the feasibility of receiving the service: security, scheduling, memory requirements, etc.

Then, the service code is coded (*e.g.* for data serialisation) for transmission on the source node, shipped through the

network, and decoded on the destination node (e.g. by using a deserialisation method).

The bandwidth required to transfer the code is equal to β_{code}, a constant, since the code size is not expected to vary during transit. Therefore, the average time required for the transmission of code (t_{code}) can be calculated by:

$$t_{code} = R\left(C_F^S, T_F^S, F_C^{code,S}()\right) + R(B_{data}, T_{data}, \beta_{code}) + R\left(C_F^D, T_F^D, F_C^{code,D}()\right) \quad (2)$$

$F_C^{code,S}()$ and $F_C^{code,D}()$ are the c.d.f. of the execution time required by the framework, on the source and destination nodes, respectively.

3) Initial state transfer

We assume that a set of *Static State Items* (*e.g.* configuration data) can be transferred prior to the quiescence of the service on the source node. After the transfer of the state items, the destination node acknowledges its reception. Consequently, the delay associated with the initial state transfer is given by:

$$t_{ist} = R\left(C_F^S, T_F^S, F_C^{ist,S}()\right) + R\left(B_{data}, T_{data}, F_C^{ist,N}()\right) + R\left(C_F^D, T_F^D, F_C^{ist,D}()\right) \quad (3)$$

where $F_C^{ist,N}()$ is the c.d.f. for the required bandwidth, $F_C^{ist,S}()$ and $F_C^{ist,D}()$ are the c.d.f. of the CPU processing time, on the source and destination node, respectively.

4) Total delay of the Preparatory phase

The time required for the *Preparatory* phase is given by:

$$t_{prep} = t_{me} + t_{dp} + t_{code} + t_{ist} - R\left(C_F^D, T_F^D, F_C^{code,D}()\right) \quad (4)$$

where t_{me} is the time that elapses from the event that triggered the mobility of a service until being received by the node responsible to determine a new system configuration. It is assumed that the new system configuration is computed in a bounded time t_{dp} [4].

It is important to note that, depending on the scenario, some of these timings can be equal to zero. As an example, assume the case where it is the user that decides to migrate its application from its mobile device to its TV, then t_{me} is equal to zero..

Most importantly, during this phase the service continues totally operational, but the characterisation of this delay is required in order to determine the dynamics of the mobility procedure.

B. Blackout Phase

1) Quiescence achieving

Usually, in reconfiguration operations, the service to be updated has to be in a safe state called quiescence [7]. In this state, the service being migrated: i) is not currently engaged in a transaction; ii) will not initiate a new transaction; iii) is not servicing a transaction; and iv) no transaction has or will be initiated by other services that require service from this service. At the same time, all services connected with the migrating service must go into a passive state, which requires the fulfilling of condition i) and ii).

One initial solution to achieve quiescence has been proposed in [7], while a less demanding solution, called tranquillity was later proposed in [8]. Achieving quiescence requires the completion of pending requests by the service being migrated and the knowledge of all other services that might issue new requests. These other services must evolve into a passive state in which they cannot evoke the service being migrated, although they can evoke other services available in the system. The time needed to achieve quiescence can be determined through a timing analysis of the mechanisms proposed in [7] or [8]. This calculation, out of the scope of this paper, is assumed to be known and equal to t_q.

We argue that achieving quiescence is not a necessary condition for the mobility of services in a distributed system, as shown by the implementation described in [9], if the service calls are stored by the mobility management and delivered to the destination node only after the completion of the mobility procedure.

2) Final state transfer

Several different approaches can be considered for state transfer: i) transfer all state in a single bundle [10]; ii) propagate only the operations done on state items [5]; iii) separate the state space into several groups of items, each transferred with its own periodicity [6] or iv) retransmit the state whenever it changes [12]. The mobility model here considered adapts to these approaches.

The final state transfer is the subphase that mostly influences the latencies of a service migration, due to its duration and due to the service being in a quiescent state (it involves the transfer of *Dynamic State Items* which can only maintain consistency if the service is not operational).

The set of state items that can only be transferred after achieving quiescence require a bandwidth of $F_C^{fst,N}()$ and CPU processing requirements of $F_C^{fst,S}()$ and $F_C^{fst,D}()$, respectively on the source and destination nodes.

CPU processing is required for the preparation of the data to be sent and the required processing time to decode the data on the destination node. Therefore, the final state transfer duration (t_{fst}) can be calculated, similarly to the case of t_{ist}, as follows:

$$t_{fst} = R\left(C_F^S, T_F^S, F_C^{fst,S}()\right) + R\left(B_{data}, T_{data}, F_C^{fst,N}()\right) + R\left(C_F^D, T_F^D, F_C^{fst,D}()\right) \quad (5)$$

3) Connections rebinding

In the migration process, connections between services need to be changed according to the new location of the migrating service.

This procedure can be performed in parallel with the *final state transfer* and it involves the exchange of messages between 2 or more nodes: the source, destination and, if any, other nodes whose services connect to the service being migrated. It mainly requires the exchange of messages containing the location of the new end points, which requires a bandwidth of β^{Si}_{reb}. Therefore, if service S_i has $ncon^{Si}$ connections with other nodes, the total bandwidth required to rebind all connections (β_{reb}) is $ncon^{Si} \times \beta^{Si}_{reb}$. The time required internally by each service to change the connection end point addresses is considered negligible.

The exchanged messages can also be used to withdraw all connected services from the passive state. Therefore, the rebinding time (t_{rbind}) is given by:

$$t_{rbind} = R\left(B_{ctrl}, T_{ctrl}, \beta_{reb}\right) \quad (6)$$

Since the number of exchanged message can be high, but with a small payload, its transmission is performed by the communication server assigned for control messages.

4) Service restart

The final subphase, which starts at the end of both the connection rebinding and final state transfer subphases, is responsible for the restart of the service on the destination node. All code and state must already be on the destination node and all necessary operations for the installation of the service (if required) have been completed. After being started, the service re-establishes its internal state using the state items previously transferred and enters full operation. This operation is performed by the service using its scheduling budget (C^D_{Si}, T^D_{Si}), and therefore the time required for service restart is given by:

$$t_{rstart} = R\left(C^D_{Si}, T^D_{si}, F_C^{rstart,D}()\right) \quad (7)$$

where $F_C^{fst,D}()$ is the p.d.f. of the CPU requirements for service restart on the destination node.

5) Total delay of the Blackout phase

During this phase, all transactions involving the migrating service are stopped, thus leading to a blackout period (t_{blk}). On a real-time system this time is particularly important since it influences the timeliness of the distributed application. Therefore, the total duration of the *Blackout* phase is given by:

$$t_{blk} = t_q + max\{t_{fst}, t_{rbind}\} + t_{rstart} \quad (8)$$

Since the final state transfer and the rebinding of connections can be executed in parallel, then we use the function $\max\{t_{fst}, t_{rbind}\}$ to determine the maximum of both subphases.

As discussed previously, the Quiescence Achieving subphase might be eliminated if the system is supported by adequate mobility management facilities. The rebinding process is based on a simple exchange of messages and on the reconfiguration of transmission and receptions ports. The service restart is an operation with a small overhead. But, the final transfer subphase delay varies with the size of the data being transferred. Particularly, when the state size is high, strategies like the ones proposed in [12] can be used in order to reduce t_{fst}. Such strategies enable the implementation of partial blocking and non-blocking approach on service calls for a migrating service.

IV. Mobility framework Architecture and Implementation

A Mobility Framework, which enables the mobility of services on the Android Operating system, has been developed. The framework will be used to demonstrate the use of the proposed model on real scenarios.

The framework is implemented as an Android service, which takes care of service migration, to and from another node, at the same time it interacts with the operating system Resource Manager in order to determine if the QoS requirements of the service can be supported.

The Android operating system is used both due to its open source nature to its innovative architecture. Although its use to support real-time applications is still debatable [15] it nevertheless provides a suitable architecture for quality of service-aware applications in ubiquitous, embedded systems [16].

The core services provided by the framework are the: *Discovery Manager*, *Package Manager*, *State Manager* and *Execution Manager*. Additionally, the framework also relies on a *QoS Manager* module that is responsible for assuring that QoS requirements of each service can be met.

The *Discovery Manager* module is designed to discover neighbour devices on a local network and advertise the host device capabilities. The advertise messages contain information about the applications and services installed, their associated *intents* interfaces and QoS requirements. Originally, Android *intents* provide the means for the reutilization of functionalities implemented by other application installed in the same device. Therefore, the *Discovery Manager* provides a standard mechanism, for each node, to obtain information about installed services and about the availability of resources in neighbour devices. It also keeps track of node and service disconnections from the network.

The *Package Manager* is used to install, uninstall and transfer the code of Android services, which are contained in *APKs* files. This module is also responsible for the interaction with the *QoS Manager* in order to request specific QoS levels for the service being handled. Therefore, its is the responsibility of the *QoS Manager* to accept or reject service installations, particularly if the QoS required level cannot be guaranteed.

The *State Manager* handles both the initial and final state transfer operations in a flexible way, based on the state items paradigm.

The *Execution Manager* allows launching services on a host device or on a remote node through the exchange of Android intents that allow the programming of transparent applications (in relation to the distribution). In this implementation an intent resolution procedure, based on the data collected by the Discovery Manager, determines if the intent can be run locally or if it must be redirected to the node, where the service is running.

The *QoS Manager* administers the system resources, either locally, on a node, or in a distributed environment. It also encapsulates the functionalities of high level QoS control frameworks, like the one defined in [4]. Consequently, this module can interact with our framework conveying orders for the deployment of services in the distributed system.

V. Conclusions and Future Work

This paper proposed a generic model for code mobility in soft real-time systems, where applications are constituted by interconnected distributed services.

The main consequence of mobility to the running application is that it might result on a temporary degradation on the provided quality of service, due to the consequent blackout period. We state that it is up to the application programmer to determine the amount of degradation that can be supported by the application. As such, this work gives the system designer the necessary tools to perform a statistical timing analysis on the execution of the mobility mechanisms and to determine the most appropriate parameters of the mobility framework modules, either in relation to the local (CPU) or to network resources.

The proposed model divides the mobility mechanism in two phases, thus allowing a reduction on the time during which a service is inaccessible (the *Preparatory* phase is not considered). This work can leverage future research in the field of code mobility and service update in distributed real-time systems. The proposed analysis can support the development and evaluation of suitable mobility mechanisms. Future work will focus on the use of the state items paradigm to propose new state transfer algorithms.

Acknowledgements

This work was supported by the ENCOURAGE project, funded by National Funds through the FCT - Portuguese Foundation for Science and Technology, as well as by the ARTEMIS Joint Undertaking, under grant agreement n° 269354.

References

[1] S. Malek, G. Edwards, Y. Brun, H. Tajalli, J. Garcia, I. Krka, N. Medvidovic, M. Mikic-Rakic, G. Sukhatme, "An Architecture-Driven Software Mobility Framework," Journal of Systems and Software, Vol. 83 Issue 6, June, 2010, pp 972-989.

[2] T. Nolte and K. Lin, “Distributed Real-time System Design using CBS-based End-to-end Scheduling,” in Proc. of the 9th International conference on Parallel and Distributed Systems, pp. 355 – 360, 2002.

[3] L. Abeni, G. Buttazzo, “Integrating multimedia applications in hard realtime systems”, in Proceedings of the 19th IEEE Real-Time Systems Symposium, Madrid, Spain, 1998, p. 4.

[4] L. Nogueira and L. Pinho, "Time-bounded Distributed QoS-Aware Service Configuration in Heterogeneous Cooperative Environments", in Journal of Parallel and Distributed Computing, Vol. 69, Issue 6, June 2009, pp. 491-507.

[5] D. Bourges-Waldegg, Y. Duponchel, M. Graf and M. Moser, "The fluid computing middleware: bringing application fluidity to the mobile Internet", in Proc. of the 2005 Symposium on Applications and the Internet, pp. 54- 63, 2005.

[6] D. Preuveneers and Y. Berbers, “Context-driven migration and diffusion of pervasive services on the OSGi framework”, in International Journal of Autonomous and Adaptive Communications Systems, Vol. 3, No. 1, pp. 33-22, 2010.

[7] J. Kramer and J. Magee, “The Evolving Philosophers Problem: Dynamic Change Management”, in IEEE Trans. on Software Engineering, Vol. 16, Issue 11 (Nov. 1990), pp. 1293-1306.

[8] Y. Vandewoude, P. Ebraert, Y. Berbers and T. D'Hondt, “An alternative to Quiescence: Tranquility”, in Proc. of the 22nd IEEE Int. Conf. on Software Maintenance, Washington, DC, (Sep. , 2006), pp. 73-82.

[9] J. Gonçalves, L. Ferreira, L. Pinho and G. Silva, “Handling Mobility on a QoS-Aware Service-based Framework for Mobile Systems”, in Proc. of the 8th IEEE International Conference on Embedded and Ubiquitous Computing (EUC 2010), Hong Kong, December 2010, to be published.

[10] M. ALRahmawy, A. Wellings, “A model for real time mobility based on the RTSJ,” in Proc. of the 5th international Workshop on Java Technologies For Real-Time and Embedded Systems (Vienna, Austria, Sep. 2007), vol. 231. ACM, New York, NY, pp. 155-164.

[11] B. K. Choi, S. Rho, R. Bettati, "Fast software component migration for applications survivability in distributed real-time systems," in Proc. of the 7th Object-Oriented Real-Time Distributed Computing, Vienna, Austria, May 2004, pp.269-276.

[12] S. Rho, R. Bettati, "Fast software component migration for applications survivability in distributed real-time systems," in Proc. of the 7th Object-Oriented Real-Time Distributed Computing, Vienna, Austria, May 2004, pp.269-276.

[13] E. Schneider, “A Middleware Approach for Dynamic Real-Time Software Reconfiguration on Distributed Embedded Systems”, PhD Thesis, Université Louis Pasteur – Strasbourg, 2004.

[14] Nogueira, L., Pinho, L., "A Capacity Sharing and Stealing Strategy for Open Real-time Systems", Published in Journal of Systems Architecture, Volume 56, Issues 4-6, April-June 2010, pp. 163-179.

[15] P. Pedreiras, P. Gai, L. Almeida, G. Buttazzo, “FTT-ethernet: A flexible real-time communication protocol that supports dynamic QoS management on ethernet-based systems”, IEEE Transactions on Industrial Informatics, vol. 1, no. 3, p. 162-172, August 2005.

[16] Maia, C., Nogueira, L., Pinho, L., “Evaluating Android OS for Embedded Real-Time Systems”, Proceedings of the 6th International Workshop on Operating Systems Platforms for Embedded Real-Time Applications (OSPERT 2010), Brussels, Belgium, 2010, pp. 63-70.

Maia, C., Noqueira, L, Pinho, L., “Cooperative embedded application in Android Environments”, Submitted for publication on the 8th International Workshop on Java Technologies for Real-time and Embedded Systems - JTRES 2010.

Evaluating the Benefits and Feasibility of Coordinated Medium Access in MANETS

Marcelo Maia Sobral
Dept of Automation and Systems
Federal University of Santa Catarina
Florianopolis, SC - Brazil
Email: sobral@das.ufsc.br

Leandro Buss Becker
Dept of Automation and Systems
Federal University of Santa Catarina
Florianopolis, SC - Brazil
Email: lbecker@das.ufsc.br

***Abstract*—A mobile ad-hoc wireless network is characterized by a highly-dynamic topology where neither the duration of links between nodes nor their density within the network can be predicted. To better understand the effect of such issues in the medium access we provide a performance evaluation of two distinct MAC protocols. The first is our previously proposed HCT (Hybrid Contention/TDMA) Real-Time MAC protocol, which continuously adapts to topology modifications to provide a kind of coordinated medium access. Its performance is compared with a contention-based, non-coordinated CSMA protocol. We compare both protocols with respect to their ability to deliver messages in a timely manner in special simulated networks scenarios that deal with mobile nodes. More specifically, we compare both the ratio of messages delivered within their deadlines and medium utilization presented by these protocols in networks with different spatial densities and speeds of nodes. Our study also analyzes the feasibility of using such adaptive protocol in respect to its overhead.**

I. Introduction

Analyzing some new-generation embedded applications one can see that they rely on mobile-connectivity. For instance, in the CarTel project [1] data is collected from sensors located on automobiles that move around the city. Modern Intelligent Transportation Systems use vehicle-to-vehicle (V2V) systems like platooning, which helps to reduce traffic congestions and provide safe driving [2]. The space community is developing distributed satellite systems (DSS) [3], where multiple mini-satellites in varying configurations are used to achieve a mission's goals collaboratively. Most of these applications require some kind of QoS guarantee in respect to the timely delivery of messages.

It happens that mobility causes topology changes and temporary link disruptions, affecting communications predictability. So the challenge in this context is how to rely on wireless links to achieve timing guarantees. This issue presents a kind of contradiction in the real-time domain, as it conflicts with the need for temporal determinism.

Several existing MAC protocols where designed to handle such mobility issues. In [4], Kumar et al presented a survey about MAC protocols used in ad-hoc wireless networks. The well known Z-MAC [5], for instance, is a dynamic protocol that adapts itself to the network conditions, using CSMA during normal workload and TDMA in high workload. Its drawback comes from the high overhead for reconfigurations (about 30s according to authors), which makes it not suitable for mobile applications. Another example is the AdHoc-MAC [6], which was conceived for inter-vehicles communication using a distributed TDMA slot allocation mechanism named RR-ALOHA. Its drawback comes from the need of configuring the application offline, making it not applicable for mobile applications.

Despite the limitations of such protocols, it is concluded that hybrid approaches to medium access are the key to achieve timely behavior in mobile networks. Inspired on that we proposed the so-called Hybrid Contention/TDMA-based (HCT) MAC [7], which aims to provide a time bounded medium access control for mobile nodes that communicate through an ad-hoc wireless network. The key issue in this protocol is to self-organize the network in groups of adjacent nodes called *clusters*, as a mean to solve the problem of timely transmission of messages. It assumes a periodic message model and a transmission cycle divided in time-slots, where each cluster reserves a predefined number of time-slots that can be assigned to its member nodes.

A. Goals and Structure of the Paper

The current paper presents and discusses results obtained from an intensive simulation study related to mobile applications that rely on timely delivery of messages. Its goal is to emphasize the benefits of having coordinated medium access to achieve the timing requirements when compared to a contention-based approach (CSMA). We also present some hints on the existing performance bounds of the protocols. To conclude, our study analyzes the feasibility of using an adaptive protocol like HCT-MAC in respect to its overhead.

In the simulations we compare both the ratio of messages delivered within their deadlines and the medium utilization presented by HCT-MAC and CSMA protocols in networks with different spatial densities and speeds of nodes.

The remainder of the paper is structured as follows: section II provides an overview of our HCT-MAC protocol. Section III details the performance parameters to be analyzed in our comparison. Section IV presents the simulation experiments performed and discusses the obtained results. Section V concludes the paper.

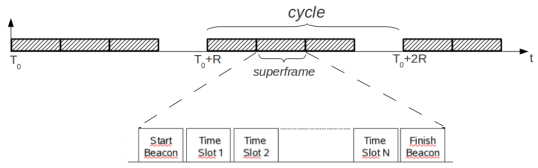

Fig. 1. Timing in HCT: cycles of length R divided in superframes

II. The HCT-MAC Protocol

In [7] we presented the Hybrid Contention/TDMA-based (HCT) MAC, which aims to provide in an opportunistic manner a time bounded medium access control for mobile nodes that communicate through an ad-hoc wireless network. It assumes that wireless links within groups of nodes can last enough to allow the use of a resource-reservation approach to medium access control, even if nodes are moving. Thus, a key issue in this protocol is to self-organize the network in groups of adjacent nodes called *clusters*, as a mean to solve the problem of timely transmission of messages.

The HCT-MAC is a hybrid protocol because it has both contention-based and resource-reservation characteristics. Contention-based access is performed with a CSMA-like MAC and resource-reservation is implemented similarly to TDMA, but constrained to the cluster and its neighborhood. Initially all nodes operate in contention-based mode and, as they succeed to form clusters, they might operate in resource-reservation mode. The timing in the HCT has a periodic and hierarchical structure, as illustrated in figure 1. A *cycle* is the basic period for transmissions, thus it works like a time unit for the protocol. It is an interval of time that is common to all clusters, and is divided in *superframes*, which are allocated by clusters. Superframes contain the same number of *time-slots*, used by the cluster members, plus two control frames called *beacons*. The predefined transmission cycle length limits the number of available superframes per cycle, and thus the number of clusters. It means that at each location in a network the number of clusters upto two hops apart is constrained by the amount of available superframes. Finally, within each cluster the allocated time-slots can be used just like in a TDMA protocol.

The TDMA component of the HCT, detailed in [8], depends on the clustering of the nodes, which must be obtained in a self-organized manner. Self-organization is a requirement because the HCT protocol was designed to be used in mobile ad-hoc networks, where nodes are not previously aware of the topology, neither of their neighborhoods. The chosen approach relies on each node performing initially a contention-based medium access and then shifting to time-based, as soon it becomes a cluster member. Nodes that are not members of cluster access the medium in a contention-based manner within unallocated superframes. In other words, as nodes self-organize in clusters they can reserve bandwidth and transmit messages in a timely manner.

In HCT-MAC clusters represent sets of nodes that agree to share a superframe, which represents a portion of the network bandwidth. It must be noted that a node can send messages to any other node within its range, since clustering has as only purpose to help nodes to allocate time-slots within a superframe. A key element in the cluster topology is the cluster-head, a special node responsible to start cluster transmissions with a start beacon, to account for idle and used time-slots, and to report successful transmissions within a finish beacon sent in the end of a superframe. Ideally, the cluster-head should be the node with the best link qualities to adjacent nodes within the region to be covered by the cluster, in order to minimize the probability of errors in transmissions in the scope of the cluster.

The clustering procedure is driven by two main guidelines: i) single nodes elect the best nodes to become cluster-heads and ii) cluster-heads choose and invite the best nodes to become cluster members. Clustering is performed continually, such that HCT can adapt to topology changes which affect links qualities between nodes.

III. Evaluation Description

The evaluation of benefits and feasibility of a HCT as coordinated MAC protocol was performed taking into account both medium utilization and timely delivery of messages provided by such protocol, and the overhead of its coordination mechanisms.

Medium utilization is a prominent result of a MAC protocol, because it informs how much of the channel capacity can be effectively used. A MAC which presents a given probability of transmission errors due to collisions cannot fully utilize the channel capacity. Moreover, in this case some messages are expected to be lost due to collisions. In fact, contention-based MACs, like the well known CSMA/CA [9], [10] and its variations, perform a probabilistic medium access and commonly use random delays before transmitting messages to reduce the probability of collisions. However, a MAC which employs some kind of coordination among transmissions of different nodes,like our proposed HCT-MAC, can improve the medium utilization. In this case, channel can be better utilized if collisions are very unlikely and random delays become unneeded.

The performance of HCT with respect to medium utilization was investigated by two metrics called i) *rate of received frames* and ii) *rate of delivered frames*. The first metric gives the ratio between the number of received frames and the maximum allowed according to TDMA. The second metric refines that measure by accounting for the successful delivered frames, which were received by nodes for whom they were addressed. When combined, these metrics can estimate how close of TDMA performance was HCT in a given scenario defined by spatial density of the network and mobility pattern.

With respect to medium utilization, HCT performance is expected to lie between a pure contention-based MAC like CSMA and a pure TDMA MAC. In case of TDMA and assuming a frame fills one time-slot entirely, if a transmission cycle T has N time-slots, a node can receive at most $N-1$ frames per cycle. In a CSMA MAC, nodes contend for the medium

and thus their transmissions are subject to collisions. If nodes transmit frames with period T using CSMA, the number of frames each node receives is expected to be smaller than $N-1$ due to collisions. Since HCT combines both medium access modes, the amount of frames each node receives should be upper bounded by TDMA and lower bounded by CSMA.

The expected enhancement in medium utilization and timely delivery of messages provided by HCT depends on the feasibility of its resource-reservation mechanisms. The resource-reservation access mode of HCT depends on the network self-organization in clusters, which occurs continually as explained in section II. Nodes form a cluster when some node is elected as cluster-head and invites other nodes to use the time-slots which are available to the cluster. Both election of cluster-head and invitation of cluster members are driven by the measured link quality estimation performed by each node, in such way a cluster can be composed by nodes with good relative links qualities. In a mobile network, links qualities change over time due to nodes movements, which implies clusters being modified or dissolved, and new clusters being formed. This way, each node can alternate intervals of time when it is member of cluster and when it waits to enter a new cluster. The metric called *clusterized rate* was defined by the average ratio of the number of clusterized cycles experienced by each node and the total number of transmission cycles. Since there is a limit in the number of possible clusters within 2 hops, the *clusterized rate* is expected to depend both on the network size and spatial density. Moreover, mobility can make clusterized intervals shorter.

Mobility in the simulated networks implies changes in clusters memberships and it means a clusterized node can leave its cluster (or even its cluster can be dissolved) and wait some time until entering a new cluster. Once outside a cluster a node cannot benefit from the contention-free medium access provided by HCT. This way, the interval of time a node is expected to wait to enter a new cluster should be known, and is defined by the metric called *disconnected time*. This metric is calculated as a cumulated probability density function which gives the probability that a node suffers a given delay to enter a new cluster.

IV. Simulation Experiments

This section presents a simulation study developed in order to provide a clear understanding on the ability of HCT-MAC protocol to utilize the medium and deliver frames within their deadlines in networks with mobile nodes, compared to a traditional CSMA protocol. It also investigated to which extent HCT was able to clusterize nodes in the simulated scenarios, which relates to the feasibility of its resource-reservation mechanism.

In our simulations we used a sort of circular mobility model, i.e., where nodes are part of a race competition. Groups of 40 to 60 nodes were disposed randomly along a circular track, moving in the same direction with speeds between 0 and 40 m/s, with a 2 m/s step. Once started a simulation, the speeds of nodes did not change. Each node periodically sent a message addressed to a neighbour which presented the best link quality in the previous transmission cycle. The resulting workload was balanced such that all nodes sent and received in average the same amount of messages.

TABLE I
General Simulation Parameters

Simulation Parameter	Value
Period of messages	48 ms
Deadline	96 ms
Maximum hops	1
Message length	16 bytes
Simulation Time	120 seconds
Mobility Model	Race (circle)
Circle Radius	from 10 upto 300 meters
Speed	from 0 upto 40 m/s
Number of Nodes	40 and 60
Sensitivity	-95 dBm
Default Transmission Power	-5 dBm
Thermal Noise	-100 dBm
Path loss exponent	2.4
Path loss at d0	55 dBm
d0	10 m

As described in table I, nodes moved along the 10 m width circular track, with radius ranged from 10 up to 150 m, in the case of networks with 40 nodes, and 30 up to 300 m in networks with 60 nodes, both using steps of 10 m. The spatial densities of the networks were calculated by the ratio between that enclosed area and the number of nodes, and was expressed as the average distance between nodes. This way it was possible to vary the spatial density of the networks and their degree of mobility. The physical layer parameters were chosen to simulate an indoor environment with no obstacles between nodes, and typical transmission range of 150 m.

As shown in table II, each transmission cycle in HCT had 6 superframes with 8 time-slots each, with time-slots lasting for 1 ms. It allowed clusters with at most 7 nodes (2 time-slots are reserved for Start and Finish Beacons, but cluster-heads use Start Beacons to encapsulate their data messages). One superframe was reserved for contention-based access, to be used by nodes which could not become members of a cluster. In that case, such nodes contended for the medium only within unallocated superframes.

Simulations were performed using the Omnet++ framework [11]. HCT model used as physical layer the radio and wireless channel models from project Castalia, maintained by the National ICT at the University of Australia [12]. They implement the signal model proposed in [13] and simulated a IEEE 802.15.4 compatible radio. These models needed to be modified to support mobility.

A. Analysis on Performance and Medium Utilization

The *rate of received frames* obtained with HCT with particular maximum speeds of nodes had a low variability in networks with both 40 or 60 nodes. In both cases, the *rate of received frames* presented similar results with different speeds (from $0m/s$ to $30m/s$) as shown in figures 2(a) and 2(b). It must be

TABLE II
HCT SIMULATION PARAMETERS

Simulation Parameter	Value
Cycle length	48 ms
Time-slot	1 ms
Superframe size	8 time-slots
Number of superframes	6

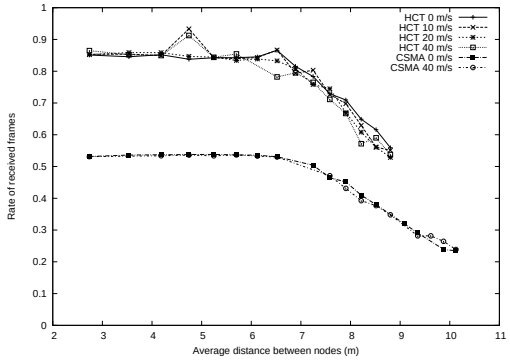

(a) Network with 40 nodes

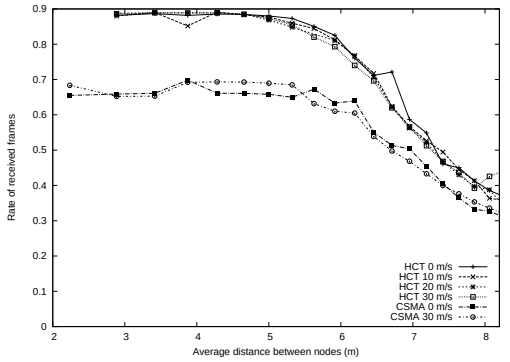

(b) Network with 60 nodes

Fig. 2. Rate of received frames

noted that in these experiments the transmission cycle of HCT would allow at most 35 nodes in resource-reservation mode in every location of the network (i.e. 5 clusters with at most 7 nodes each, since one superframe was reserved to contention-based access). Therefore, in networks with 40 nodes almost every node could clusterize and operate in resource-reservation mode even in higher spatial densities, but in networks with 60 nodes this was not true unless the spatial density corresponded to neighborhood sizes around 35 nodes. It can be clearly seen that HCT outperformed CSMA as spatial density increased (i.e. as average distance between nodes decreased). In this case, as nodes got closer their neighborhood sizes increased, leading to a higher probability of collisions in CSMA. Since HCT organizes as many nodes as possible in clusters to perform a short-range resource reservation, these clusterized

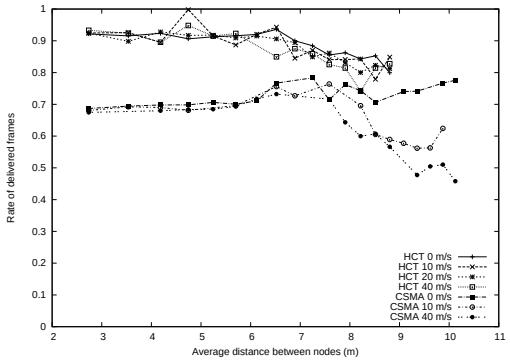

(a) Network with 40 nodes

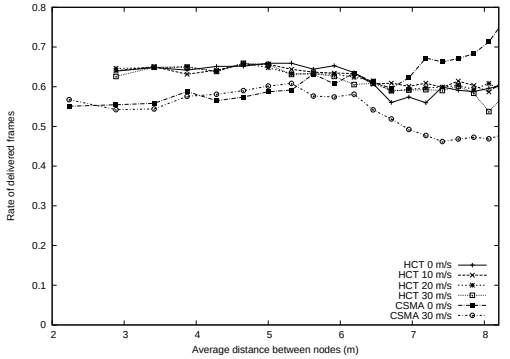

(b) Network with 60 nodes

Fig. 3. Delivered messages

nodes could transmit without incurring in collisions. The figures show also that as spatial density decreased CSMA performance approached HCT. This can be related to the smaller resulting neighborhood sizes, which resulted in lower probability of collisions if CSMA was used. Finally, since CSMA does not perform any resource-reservation nor self-organization, it must be little affected by speeds of nodes as confirmed in the figures. A similar result was obtained for the *rate of delivered frames*, which accounts for the received frames which were actually addressed to receiving nodes.

The *rate of delivered frames* relates the amount of delivered frames to the number of generated data frames throughout the network. As shown in figure 3(a), HCT presented a significantly higher *rate of delivered frames* than CSMA in networks with 40 nodes, when higher spatial densities were considered. The variability of this *rate of delivered frames* did not present a significant dependence to speeds of nodes in the case of HCT, but with CSMA the results for lower spatial densities were better with lower speeds. In networks with 60 nodes, shown in figure 3(b), HCT still outperformed CSMA in higher spatial densities but with a smaller difference.

The results obtained for *rate of received frames* and *rate of delivered frames* showed that HCT presented a better medium

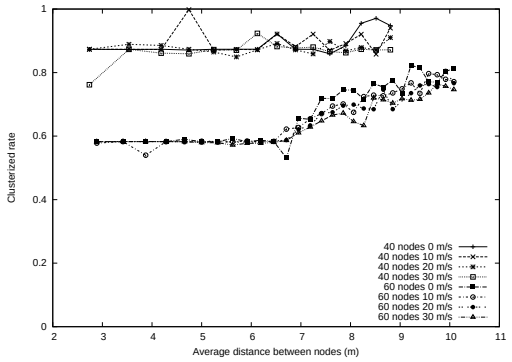

Fig. 4. Clusterized rate

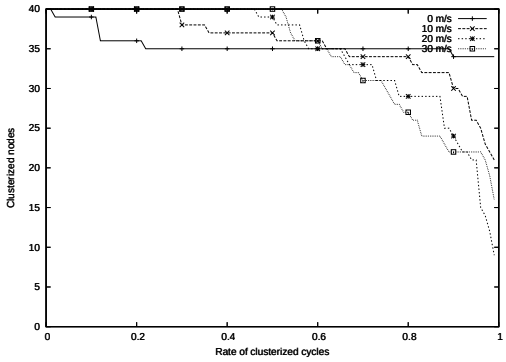

(a) Network with 40 nodes

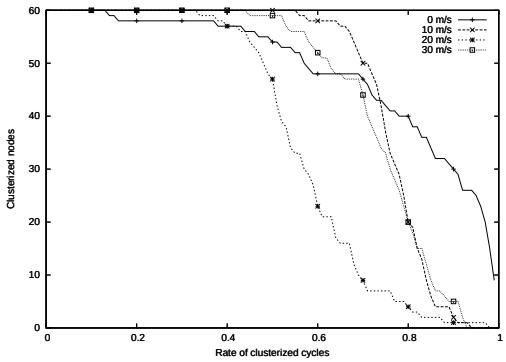

(b) Network with 60 nodes

Fig. 5. Nodes with at least a given clusterized rate

utilization than CSMA. It also showed that in some scenarios HCT approached the performance that a TDMA MAC would provide with respect to medium utilization. The better performance of HCT can be related to its resource-reservation access mode, which allows node to obtain exclusive access to the medium in a contention-free manner. Since the self-organization capability of HCT is the key to its resource-reservation mode, the next section investigates to which extent HCT was able to self-organize the networks in the simulated scenarios.

B. Analysis on Network Self-organization

In this section it is investigated the self-organization of the simulated networks, to measure the number of cycles nodes were able to stay clusterized in the different scenarios, and how long nodes must wait to enter a new cluster.

The *clusterized rate* was calculated for each simulation run of networks with 40 and 60 nodes, as shown in figure 4. It can be seen that in networks with 40 nodes the *clusterized rate* was quite steady and did not vary significantly with speed. In this case, most of nodes could clusterize since at most 5 clusters within 2 hops, with 7 nodes each, can be formed. This way, even in scenarios with high spatial densities almost all nodes were clusterized. But in networks with 60 nodes a proportionally smaller number of nodes could clusterize in high spatial densities. The *clusterized rate* in those networks remained steady in denser scenarios, and increased as the spatial density decreased enough to allow more clusters to be formed (but restricted to the defined limit within 2 hops around each cluster).

The *clusterized nodes* gives the number of nodes which presented at least a given number of clusterized cycles. It was calculated considering networks where the spatial density allowed a high *clusterized rate*. In networks with 40 nodes and average distance of $7.8m$ between nodes, shown in figure 5(a), the *clusterized nodes* had a clear dependence with speed. The figure shows that there was a threshold in the *clusterized rate* above which *clusterized nodes* suddenly and steadily decreased. Despite that, many nodes could stay clusterized almost all the time. When networks with 60 and average distance of 10 m between nodes were considered, the threshold in the *clusterized rate* appeared earlier and the steepness of *clusterized nodes* decay was more intense. In fact, in networks with 60 nodes few nodes were able to stay clusterized all the time. If *clusterized rate* and *clusterized nodes* reflects how many of the total transmission cycles correspond in average to clusterized cycles, it lacks the information about how long a node is expected to wait before becoming a cluster member.

In the case of networks with 40 nodes, it can be expected a short *disconnected time*, since almost all nodes were clusterized during the simulations, as shown in figure 6(a). It corresponds to a scenario where nodes were distant each other $4.7m$ in average, and the network had a high *clusterized rate*. It can be seen that once a mobile node left a cluster, it was very likely that it entered a new cluster within $200ms$ (which corresponded to about 4 transmission cycles in the experiments). In networks with 60 nodes, with average distance of $10m$ between nodes which resulted in a reasonable *clusterized rate*, it can be expected a longer *disconnected time* as shown in figure 6(b).

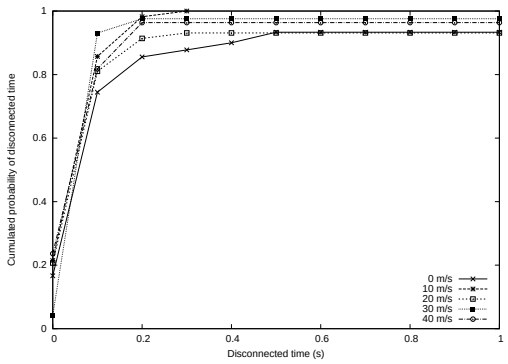

(a) Network with 40 nodes

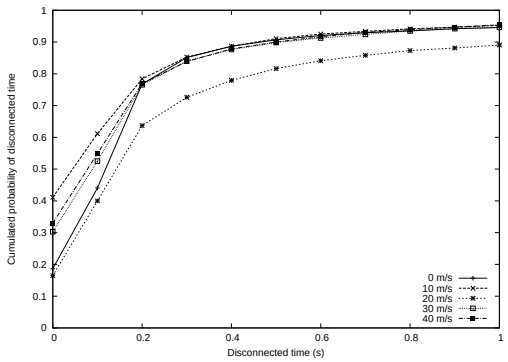

(b) Network with 60 nodes

Fig. 6. Disconnected time

V. Conclusions

The current paper presented and discussed results obtained from an intensive simulation study to investigate the use of a coordinated MAC protocol by mobile applications that rely on timely delivery of messages. The study investigated at which extent the HCT MAC protocol, which provides a coordinated medium access, would improve the medium utilization and timely delivery of messages in scenarios with mobile nodes, compared to a traditional CSMA MAC protocol.

Simulation results showed that HCT outperformed CSMA in scenarios with different network sizes, spatial densities and speeds of nodes. Despite its overhead due to network self-organization and control frames, HCT still presented a higher medium utilization and rate of successfully delivered messages compared to CSMA. Moreover, in scenarios where HCT was able to keep almost the whole network self-organized, it approached the performance it would be expected from a TDMA-like MAC protocol. However, in networks with large spatial densities its performance was similar to CSMA.

The better performance on medium utilization and timely delivery of messages of HCT can be related to its resource-reservation access mode. That was analysed on the experiments on network self-organization, which gave the ratio of nodes which were able to clusterize and thus to operate in resource-reservation mode. These results showed that the ratio of clusterized cycles each node experienced during the experiments was related to the spatial distribution of nodes in the experiemnts, but there was no clear dependence on speeds of nodes. However, speeds influenced the time that nodes were expected to wait to become cluster members.

There still exist a number of questions regarding the performance of the HCT MAC protocol regarding the chosen metrics. It must be further clarified the the dependence of its performance on spatial distribution of nodes and mobility pattern. Therefore, a desired result is to predict its performance according to such characteristics of the network.

References

[1] B. Hull, V. Bychkovsky, Y. Zhang, K. Chen, M. Goraczko, A. K. Miu, E. Shih, H. Balakrishnan, and S. Madden, "Cartel: A Distributed Mobile Sensor Computing System," in *4th ACM SenSys*, Boulder, CO, November 2006.

[2] J. Voelcker, "Cars Get Street Smart," *IEEE Spectrum*, vol. 44, no. 10, pp. 16–18, Oct. 2007.

[3] C. P. Bridges and T. Vladimirova, "Agent Computing Applications in Distributed Satellite Systems," in *9th International Symposium on Autonomous Decentralized Systems (ISADS 2009)*, Athens, Greece, 2009.

[4] S. Kumar, V. S. Raghavan, and J. Deng, "Medium Access Control Protocols for Ad Hoc Wireless Networks: A Survey," *Ad Hoc Networks*, vol. 4, no. 3, pp. 326–358, 2006.

[5] I. Rhee, A. Warrier, M. Aia, and J. Min, "Z-MAC: A Hybrid MAC for Wireless Sensor Networks," in *SenSys '05: Proceedings of the 3rd international conference on Embedded networked sensor systems*. New York, NY, USA: ACM Press, pp. 90–101.

[6] F. Borgonovo, A. Capone, M. Cesana, and L. Fratta, "AdHoc MAC: New MAC Architecture for Ad Hoc Networks Providing Efficient and Reliable Point-to-Point and Broadcast Services," *Wirel. Netw.*, vol. 10, no. 4, pp. 359–366, 2004.

[7] M. M. Sobral and L. B. Becker, "A Wireless Hybrid Contention/TDMA-Based MAC for Real-Time Mobile Applications," in *ACM Symposium on Applied Computing 2008, Real-Time Systems Track*, Fortaleza, Brazil, March 2008.

[8] M. M. Sobral and L. B. Becker, "Towards a Clustering Approach to Support Real-Time Communication in Ad-Hoc Wireless Networks," in *Brazilian Workshop on Real-Time Systems 2009 (WTR 2009)*, Recife, Brazil, May 2009.

[9] IEEE, *802.15.4: Wireless Medium Access Control (MAC) and Physical Layer(PHY) Specifications for Low-Rate Wireless Personal Area Networks (LR-WPANs)*, 2006th ed., IEEE Computer Society, 3 Park Avenue, New York, NY, USA, October 2006.

[10] IEEE, *802.11e: Wireless LAN Medium Access Control (MAC) and Physical Layer(PHY); Ammendment 8: Medium Access Control (MAC) Quality of Service*, 2005th ed., IEEE Computer Society, 3 Park Avenue, New York, NY, USA, October 2005.

[11] A. Varga, "The Omnet++ Discrete Event Simulation System," in *Proceedings of the European Simulation Multiconference*. Prague, Czech Republic: SCS – European Publishing House, June 2001, pp. 319–324.

[12] H. N. Pham, D. Pediaditakis, and A. Boulis, "From Simulation to Real Deployments in WSN and Back," in *IEEE International Symposium on World of Wireless, Mobile and Multimedia Networks, 2007. WoWMoM 2007*, June 2007, pp. 1–6.

[13] M. Zuniga and B. Krishnamachari, "Analyzing the Transitional Region in Low Power Wireless Links," in *Sensor and Ad Hoc Communications and Networks, 2004. IEEE SECON 2004. 2004 First Annual IEEE Communications Society Conference on*, pp. 517–526.

Time Constrained FlexRay Static Segment Scheduling

Zdeněk Hanzálek, David Beneš
Department of Control Engineering
FEE, Czech Technical University in Prague
Prague, Czech Republic
Email: {hanzalek,benesda1}@fel.cvut.cz

Denis Waraus
Department of Measurements
FEE, Czech Technical University in Prague
Prague, Czech Republic
Email: warauden@fel.cvut.cz

***Abstract*—The objective of the paper is the formulation and solution of the frame packing and scheduling problem for the static segment with respect to AUTOSAR FlexRay COM stack. There are several other works on the static segment scheduling. The problem becomes more constrained since the offsets and deadlines of the signals are taken into account. While assuming offsets and deadlines to be multiples of the cycle length, a solution of the scheduling problem is based on decomposition to separate nodes. The article shows simple and efficient scheduling algorithm, its evaluation on benchmarks with up to 3000 signals per node and simple experiment on real FlexRay HW.**

***Keywords*-scheduling; time-triggered communication protocols; FlexRay;**

I. Introduction

The FlexRay [4] protocol seems to establish a new standard in automotive and together with recent automotive protocols such a CAN, MOST and LIN will form a robust platform for modern cars with x-by-wire systems. BMW, the pioneer in innovative technology, uses the new protocol in their latest model for transmission of large quantities of data within the active chassis system.

Communication protocol can offer different number of the static slots based on its configuration. Nowadays, luxury cars contains up to 70 electronic control units (ECU), which require transmission up to 2500 different signals [1]. Hence, it is essential to develop a powerful algorithm for a frame packaging and scheduling with user defined constrains (signal period, offset, and deadline). In this paper, time window is we considered for each signal given by offset and deadline related to the start of the hyperperiod.

II. FlexRay overview

The FlexRay is a time-triggered communication protocol where the data transmission is based on recurring communication cycle which is composed of static segment, dynamic segment, symbol window and network idle time. The example of communication cycle is depicted in Figure 1.

The static segment comprises a fixed number of equally sized time division multiple access (TDMA) static slots. The segment is designed for frames where predictable frame delay is defined. In each static slot a frame (with a unique identifier frameID) can be transmitted by a node. Once a static slot with a unique identifier is allocated to a specific node, only this node is allowed to transmit during this slot and so protocol ensures collision avoidance. In order to ensure proper slot timing, each single node provides synchronization by synchronization frames - frame where synchronization bit is set. Synchronization is embedded in the standard and is based on differences between real and predicted frame receptions.

The dynamic segment employs the flexible TDMA approach and is intended for the non-critical and sporadic messages with varying length. The symbol window is designed for transmission of protocol symbols used for network wake-up, start-up and testing. The part of time-base correction is performed during the network idle time. The dynamic segment and symbol window are optional part of the communication cycle. The frame scheduling on the dynamic segment (see [10], [9]) is out of the scope of this study.

The frame includes previously mentioned frameID which matches to slot identifier in the static segment and the cycle number identification. There are 64 different cycles and up to 2047 static slots. The FlexRay network (cluster) can be arranged in different physical topologies such as a star, a bus, a point-to-point or a hybrid topology. Two independent physical channels should be preferably used for high bitrate or enhanced safety. Every single channel can form a different physical topology. In this paper, it is assumed, that the same data are transmitted on both channels.

III. Related work

The goal of the paper is the formulation and solution of the frame packing and scheduling problem for the static segment with respect to AUTOSAR FlexRay COM stack. There are several other works on the static segment scheduling. Techniques for determining the timing properties of messages transmitted in both the static and the dynamic segments of a FlexRay communication cycle are proposed in [9]. The analysis techniques for messages are integrated in the context of a holistic schedulability analysis that computes the worst-case response times of all the tasks and messages in the system. Authors present and evaluate three optimization algorithms that can be used to improve the schedula-

bility of a system that uses FlexRay. Unfortunately, authors assume knowledge of all signals in system for bandwidth optimization by modification of protocol parameters such as number of static slots, static and dynamic segment duration. The assumption is quite limiting for automotive industry applications where an incremental design is commonly used.

A mathematical model determining the optimal length of static messages that can achieve more efficient use of a FlexRay is presented in [12]. However, knowledge of all signals in a system is once again required. Moreover, the longest high priority frames are reallocated to the dynamic segment and thus system have to be redesigned with each extension; otherwise it cannot be guaranteed that frames in dynamic segment meet deadlines.

The message frame packing that maximizes network efficiency by reducing unused slots is investigated in [11]. Signals are packed into the same size messages to obey the restrictions of the FlexRay protocol, while narrow bandwidth is used. Then authors formulate a nonlinear integer programming problem to compute an optimal message set from given set of signals. They also proposed a scheduling method with low jitter and minimum number of static slots to improve the network efficiency. In contrast to [11], the offsets and deadlines of the signals are taken into consideration in this paper, so the problem becomes more constrained.

The authors of [5] assume usage of AUTOSAR COM stack and use heuristic analysis to schedule relatively large message set. The authors assume that frame packing is done by the application level.

An optimization framework that includes not only signal to frame packing, but also frame to slot assignment, task schedule and the synchronization of signal and task scheduling considering end-to-end delays and the precedence constraints induced by information passing between tasks and signals is presented in [13]. Presented mixed-integer linear programming formulation includes the system-level schedule optimization with the definition of an optimal relative phase in the activation of tasks and signals which accounts for deadlines and precedence constraints. Moreover, usage of AUTOSAR standard is assumed, but framework is evaluated only on typical X-by-wire application.

IV. Problem Statement

Two sets of tasks executed in ECUs are to be considered: the first set contains tasks that are running without synchronization with communication cycle. Signals (ie. communication of one state variable from one ECU) generated by these tasks are called *asynchronous signals*. Signals provided by the second set of task which are synchronized with communication cycle are called *synchronous signals*. The objective is to find packing of signals into frames and allocation of frames to specific slot and cycle.

FlexRay network configuration consists of large parameter set including a cycle length, number of static slots in the

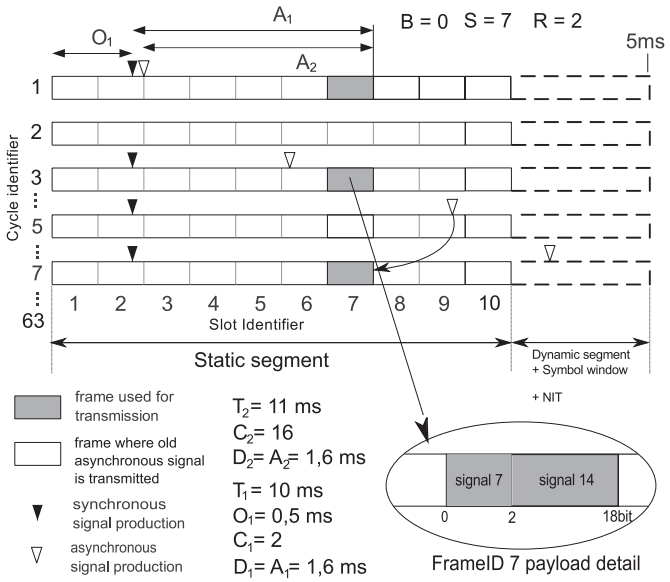

Figure 1. Illustration of generation of synchronous and asynchronous signals

static segment, duration of static slot, duration of NIT segment etc. These parameters are usually predefined by system designer and further followed by ECU suppliers. The following setting based on the BMW network design [2] is used in this paper. The communication cycle duration is equal to F = 5 ms where static segment takes 3 ms and the rest of the communication cycle is filled by the dynamic segment, symbol window and network idle time. There are M = 75 static slots with static slot duration of L = 0,04 ms. The frame payload W = 128 bits.

For each single signal an user can define the following parameters (we use same denotation with [5]):

- N_i unique identifier of ECU, which transmits the signal *i*,
- T_i signal period *i*, the signal is assumed to be transmitted only once in Flexray cycle,
- O_i is the signal offset, it is the latest time after which the first occurence of the signal is produced in relation to the start of period,
- C_i signal *i* size in bits,
- A_i the signal age is the duration between the signal production at the sender side and the end of the first frame carrying the signal on receiver side.
- D_i is the deadline associated to the signal *i*, it represents the maximum age acceptable at the consumer end.

Next assumption is usage of AUTOSAR communication stack[8] which is de facto standard for automotive applications and it is considered also for other industry applications such as aviation. In this context, the AUTOSAR frame is defined by

Q_j unique ECU identifier, which transmits the frame *j*,

S_j static slot identifier used for frame *j*,

R_j the AUTOSAR frame repetition, which is the transmission period of frame expressed as a multiple of the communication cycle with the constrains that the repetition takes its value in $\{2^n | n \in \mathcal{N}, n \leq 6\}$,

B_j the base cycle identifier - the first occurence of the frame *j*. $B_j \leq R_j$.

Each single frame *j* is thus characterized by a tuplet $\{Q_j, S_j, B_j, R_j\}$. The frame contains processing data units (PDU) where each consists of one or more signals. An *update bit* can be defined for each PDU. It informs recipients whether at least one signal in the PDU was updated or not. The signal can be contained in more than one PDU. In AUTOSAR context is defined that scheduling is static and cannot be changed during runtime.

It is further assumed, that maximal signal size cannot exceed data payload of the frame. It means that signal cannot be split into two or more frames. Message fragmentation is ensured by AUTOSAR FlexRay transport protocol layer [7].

By oversampling, the asynchronous signal is transformed to synchronous one with the following parameters:

$$\begin{aligned} D_i = T_i &= 2^n \cdot F + P + U \\ O_i &= 0 \end{aligned} \tag{1}$$

where P is packing time - time from task request on signal *i* transmission to the start of frame transmission and U is unpacking time.

Synchronous signals can keep deadline shorter than a period. In this case deadline is limited by the following values

$$D_i^S \geq \begin{cases} P + L + U \text{ for } \quad 0 \leq O_i - n \cdot F \leq P + M \cdot L + U \\ P + L + G + U \text{ otherwise} \end{cases} \tag{2}$$

where $n \in 1, 2, ..64$, M is number of static slots, L is duration of the static slot, and G is duration of dynamic segment, network idle time and symbolic window.

The Figure 1 depicts a situation where two signals are generated – synchronous one and asynchronous one. The period of synchronous is set to 10 ms and 11 ms for asynchronous. Let us assume that, both signals have the deadline equal to the period. In order to fulfill the deadline constraint, it is necessary to transmit both signals every second cycle, it means $R_j = 2^1$. In the fourth cycle ECU transmits the same data twice due to oversampling of the asynchronous signal. However, this behavior is covered by previously mentioned *update bit*.

A. Message set

The scheduling approaches are applied to the modified Society of Automotive Engineers (SAE) benchmark signal set.

The SAE report describes a set of signals sent between seven different subsystems in an electric car prototype. The Basic SAE signal set defines 53 sporadic and periodic signals. A periodic message has a fixed period 5, 10, 100, 1000 ms, and implicitly requires the latency to be less than or equal to this period. Sporadic messages have latency requirements imposed by the application: for example, all messages sent as a result of a driver action have a latency requirement of 20 ms. The reader is referred to the work of Kopetz [6] for more detailed benchmark description. Due to the high FlexRay bandwitch (10Mb/s) and electronic equipment's requirements in today's cars we extended the SEA benchmark using NETCARBENCH[3] to:

- increase the number of signals while using the same probability distribution function of parameters - up to 3000 signals per node are considered in this article,
- add parameters (such as offset).

B. Time constraints

In the first step, it is needed to find each signal pair $\{E_i, H_i\}$ where E is earliest and H latest slot which can be used for transmission of the first occurrence of the signal *i*. The pair is given by

$$\begin{aligned} E_i &= floor(\frac{P + O_i}{F}) \cdot M + \\ &+ min \quad (ceil(\frac{(P + O_i - floor(\frac{P+O_i}{F}) \cdot F}{L}), M) \end{aligned} \tag{3}$$

$$\begin{aligned} H_i &= floor(\frac{P + O_i}{F}) \cdot M + \\ &+ min \quad (floor(\frac{P + O_i + D_i - floor(\frac{P+O_i}{F}) \cdot F}{L}), M) \end{aligned} \tag{4}$$

In order to simplify the scheduling problem, each node is scheduled separately, following decomposition in [11]. For this reason, we express $\{\tilde{O}_i, \tilde{D}_i\}$, earliest and latest cycle to transmit signal i, as follows:

$$\tilde{O}_i = ceil(\frac{E_i}{M}) \tag{5}$$

$$\tilde{D}_i = floor(\frac{H_i}{M}) \tag{6}$$

This simplifies our scenario, since offsets and deadlines could be only multiples of the cycle length, because position of signal within the cycle is insignificant with respect to position of signal within hyperperiod. This effectively means, that we don't care about assignment of particular ID to the node, so it is not important, that the node has the first ID, or the last one.

V. Algorithm

The Time Constrained FlexRay Static Segment Scheduling (TCFSSS) algorithm could be shortly described in pseudo code of Algorithm 1 where $schedule$ is the actual ID, cycle and offset in the frame, when signal will be first send over the network.

Input: C, T, $\tilde{O}$, $\tilde{D}$
Output: $schedule$

$[signals_{node_1}, ..., signals_{node_{number\,of\,nodes}}] =$
$= divide\,signals\,to\,nodes(C, T, \tilde{O}, \tilde{D})$
$for\,(k = 1 ... number\,of\,nodes)\,do:$
$messages_{node_k} = frame\,packing(signals_{node_k})$
$opt\,messages_{node_k} = optimization(messages_{node_k})$
$schedule_{node_k} = create\,schedule(opt\,messages_{node_k})$
$schedule = [schedule_{node_1}, ..., schedule_{node_{number\,of\,nodes}}]$
$if\,(schedule.slots > M)$
$error('Could\,not\,find\,correct\,schedule')$

Algorithm 1: Pseudo code of the TCFSSS algorithm

A. Divide signals to nodes

Due to the fact that offsets and deadlines are multiples of cycle length, it is not needed to decide which node should have lover IDs than the others and this leads us to the possibility to compute schedules separately for each node. Therefore signal are simply divided into the sets according to the node that send the signal. This is performed in asymptotic time complexity $O(S)$ where S is the number of the signals on the input.

Above means, that our algorithm is able to take advantage of parallel processing on multiple processors. After dividing signals, algorithm could be split into independent parts for each node. When branches successfully finishes their computation, final result is obtained just by putting individual results consequently one after another.

B. Frame packing

The idea of frame packing is described in [11]. Frame packing is done separately for each period of signals. Frame packing groups signals into messages that are not larger than the slot and have all properties as a signal, it has the same period T_i as signals packed into this message, size C_i as a sum of the sizes of individual signals in the message and also computed offset $\tilde{O}_i$ and deadline $\tilde{D}_i$ from those signals.

	C_i	T_i	$\tilde{O}_i$	$\tilde{D}_i$
s_1	26	2	0	2
s_2	2	1	0	1
s_3	2	4	0	11
s_4	6	4	0	13
s_5	6	8	1	8
s_6	8	1	0	1
s_7	2	2	0	2
s_8	4	1	0	1
s_9	32	8	5	8
s_{10}	16	2	1	2
s_{11}	4	4	0	9
s_{12}	14	1	0	1
s_{13}	4	1	0	1
s_{14}	16	2	0	1
s_{15}	10	16	1	6
s_{16}	8	2	0	2
s_{17}	4	2	0	2
s_{18}	2	8	3	7
s_{19}	14	16	1	16
s_{20}	20	1	0	1

Table I
Signals on the frame packing input for one node ($signals_{node_7}$)

The message simply groups the signals to simplify scheduling by while reducing the number of elements that need to be scheduled. When searching for the message, where given signal can be placed, only messages with the same period, which has enough free space are taken into account. That means, that size of the message with the size of the added signal could not be larger than the size of the slot. Furthermore, to fit signal into message, offset of the message must be equal or larger than the offset of the signal and message deadline must be shorter than or equal to the signal deadline.

When the signal is added in the message, offset and deadline of the message must be adjusted to fulfill constrains of all signals in the message. If no convenient message (message without enough free space or message, that doesn't satisfy all the constraints) for specified signal is found, new message with given signal's properties (size C_i, period T_i, release time $\tilde{O}_i$ and deadline $\tilde{D}_i$) is created. As an example of frame packing, see Table I which shows input signals for one node. During this part of the algorithm for the input signals in Table I, signals were converted into messages depicted in the Table II.

	C_i	T_i	$\tilde{O}_i$	$\tilde{D}_i$	signals
m_1	32	1	0	1	s_2, s_6, s_8, s_{12}, s_{13}
m_2	20	1	0	1	s_{20}
m_3	30	2	0	1	s_7, s_{14}, s_{16}, s_{17}
m_4	26	2	0	2	s_1
m_5	16	2	1	2	s_{10}
m_6	12	4	0	4	s_3, s_4, s_{11}
m_7	8	8	3	7	s_5, s_{18}
m_8	32	8	5	8	s_9
m_9	32	16	1	6	s_{15}, s_{19}

Table II
Messages created during frame packing for one node ($messages_{node_7}$)

Frame packing is computed in asymptotic time complexity $\mathcal{O}(s^2)$ where s is number of the signals of the given node.

C. Optimize messages

Most likely, not all of the messages would have exactly the size of the slot, so there is another step, which tries to

use the empty space in messages for messages, that can fit into the free space and have lower periodicity. Therefore we reduce the number of messages that need to be scheduled, so it can cause reduction of the number of needed IDs allocated to the node.

This is obtained by iterating over all messages (notice, that previous part of the algorithm was performed separately by periods, but this part works on all messages of the node) sorted from the least occurring message to the most occurring one. Each message is checked, if it couldn't be merged with some other message for current node with preserving it's constrains. Sorting messages from the least occurring to the messages with highest periodicity reduces the amount of old unneeded data (data sent more frequently, than is it's periodicity) sent over the network, in the other words algorithm tries to reach the best possible effectivity. Pseudo code of the described method is depicted in Algorithm 2.

Input: $messages_{node_k} = [m_1, ..., m_{number\,of\,messages_{node_k}}]$
Output: $opt\,messages_{node_k} = [m'_1, ..., m'_{number\,of\,optimized\,messages_{node_k}}]$

$for\,(p = 1 \ldots number\,of\,messages_{node_k})\,do:$
  $m'_p = m_p$
  $for\,(q = (p+1) \ldots number\,of\,messages_{node_k})\,do:$
    $if\,(m'_p\,can\,be\,merged\,with\,m_q)$
      $m'_p = merge\,m'_p\,and\,m_q$
      $delete\,m_q$
    $endif$

Algorithm 2: The idea of the message optimization part of the algorithm for node k

See Table III for the output of the message optimization part of the TCFSSS alogirithm.

	C_i	T_i	O_i	D_i	messages
m'_1	32	1	0	1	m_1
m'_2	20	1	0	1	m_2
m'_3	30	2	0	1	m_3
m'_4	26	2	0	2	m_4
m'_5	28	2	1	2	m_5, m_6
m'_6	32	8	3	6	m_7, m_9
m'_7	32	8	5	8	m_8

Table III
OPTIMIZED MESSAGES CREATED DURING THE MESSAGE OPTIMIZATION FOR ONE NODE ($optimized\,messages_{node_7}$)

To meet all constrains of original signals, latest offset and earliest deadline must have been chosen.

Optimization of the messages is done in asymptotic time complexity $\mathcal{O}(m^2)$ where m is the number of the messages from the previous step of the given node.

D. Create schedule

Messages are being scheduled from the most frequent messages to the messages with the longest period. For each message, the algorithm tries to find the ID, which has enough of the free space (empty frames in the cycles of the hyperperiod) and meets all requirements (offset and deadline of the message).

This process is very similar to the frame packing. The messages are separated for suitable position in those IDs which have enough of free space, in this search we consider only the cycles that meet offset and deadline of the message. If proper position is found, it's place is recorded to the message and corresponding cycles are marked (because message generally occupies more frames thanks to it's periodicity) as occupied. If no suitable ID could be found, new ID is reserved, and message is placed into this one and occupied cycles are marked in the same way.

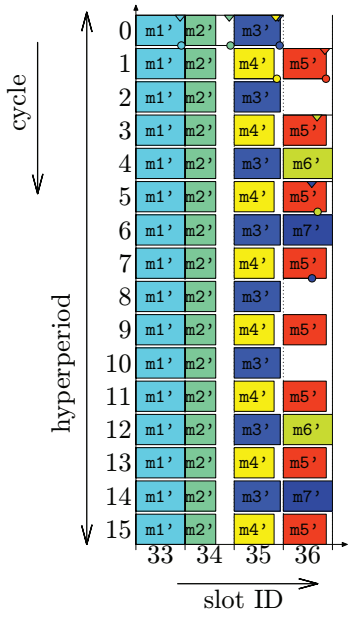

Figure 2. Final computed schedule for one node ($schedule_{node_7}$)

Final computed schedule is shown on the Figure 2. It shows, that 20 signals on the input of the algorithm could be scheduled into 4 slots. At the beginning, signals requested to transfer 1560 bits of information during the hyperperiod. Thanks to the optimization part, in the final schedule, node needs to transfer 1632 bits of the information, so our optimization overhead is in this case 4.6%. In those 4 slots it is possible to transfer at most 2048 bits, that means, that this example use nearly 80% of the available bandwidth.

Creation of schedule is done in asymptotic time complexity $\mathcal{O}\left(max(m' \cdot i \cdot c,\, m' \cdot log(m'))\right)$ where m' is the number of the optimized messages for the given node, i is the number of the IDs associated to the given node and c is the number of cycles in the hyperperiod. $m' \cdot log(m')$ stands for the sort complexity, because optimized messages must be sorted on the input of this part of the algorithm.

VI. PERFORMANCE EVALUATION AND CONCLUSION

Computing time of the algorithm mainly depends on the maximum number of signals for a node. The TCFSSS

# of signals	696	775	973	2667
# of nodes	3	6	1	1
Overhead	5.24%	6.42%	0.54%	0.60%
Utilization	91.74%	82.68%	97.78%	98.05%
Computation	0.84s	0.62s	0.87s	2.10s

Table IV
PERFORMANCE OF TCFSSS ALGORITHM

algorithm was tested on signal sets with three nodes and about 700 signals generated by netcarbench and it is able to compute schedule in about 8 seconds when one node had 400 signals in those signal sets. For signals sets with only one node, but with about 3000 signals per node, takes TCFSSS algorithm about 35 seconds to compute the schedule. Performance was measured on single core Intel 2.4GHz processor and 1GB of RAM, using Matlab R2009B on Windows XP.

Overall time complexity of the TCFSSS algorithm is $\mathcal{O}\left(S + n \cdot (s_n^2 + m_n^2 + max(m'_n \cdot i_n \cdot c,\, m'_n \cdot log(m'_n)))\right)$ in the worst case scenario, where S is the overall number of the signals on the input, n is the number of the nodes, s_n is the number if the signals of the given node, m_n is the number of the messages of the given node, m'_n is the number of the optimized messages of the given node, i_n is the number of IDs assigned to the given node and c is the number of the cycles in hyperperiod.

Table IV illustrates time complexity of the algorithm for different number of signal. The values of utilization illustrate efficiency of this algorithm. The computation time leaves the room for further extensions of the algorithm.

In order to verify the schedule shown in this paper, a simple experiment have been conducted with real FlexRay HW based on Freescale MC9S12XF and Tektronix oscilloscope MSO/DPO4000B Series. Part of one communication cycle (separate lines represent separate signals) is shown on Figure 3.

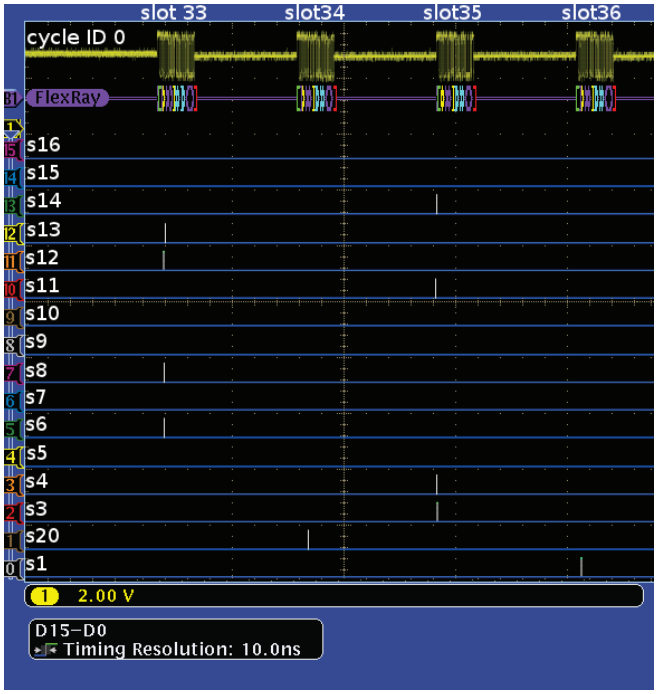

Figure 3. Experiment on real HW

REFERENCES

[1] Amos Albert. Comparison of event-triggered and time-triggered concepts with regard to distributed control systems. In *Embedded World 2004*, pages 235–252, 17.–19.02.2004 2004.

[2] Josef Berwanger, Martin Peteratzinger, and Anton Schedl. Flexray startet durch – flexray-bordnetz får fahrdynamik und fahrerassistenzsysteme. *In Elektronik automotive: Sonderausgabe 7er BMW*, 2008.

[3] Christelle Braun, Lionel Havet, and Nicolas Navet. Netcarbench: A benchmark for techniques and tools used in the design of automotive communication systems. In *The 7th IFAC International Conference on Fieldbuses and Networks in Industrial and Embedded Systems (FeT'2007)*, November 2007.

[4] FlexRay Consortium. Flexray protocol specification v2.1 rev. a, 2005.

[5] Mathieu Grenier, Lionel Havet, and Nicolas Navet. Configuring the communication on FlexRay: the case of the static segment. In *Embedded Real Time Software*, France, 2008.

[6] H. Kopetz. A solution to an automotive control system benchmark. In *Real-Time Systems Symposium, 1994., Proceedings.*, pages 154 –158, 7-9 1994.

[7] AUTOSAR Development Partnership. Specification of flexray transport layer. Version 2.0.1, June 2006.

[8] AUTOSAR Development Partnership. Specification of module flexray interface. Version 2.0.0, June 2006.

[9] T. Pop, P. Pop, P. Eles, Z. Peng, and A. Andrei. Timing analysis of the flexray communication protocol. *Real-Time Systems, 2006. 18th Euromicro Conference on*, pages 11 pp.–216, 2006.

[10] E. G. Schmidt and K. Schmidt. Message scheduling for the flexray protocol: The dynamic segment. *Vehicular Technology, IEEE Transactions on*, 58; 58(5):2160–2169, 2009.

[11] K. Schmidt and E. G. Schmidt. Message scheduling for the flexray protocol: The static segment. *Vehicular Technology, IEEE Transactions on*, 58; 58(5):2170–2179, 2009.

[12] Byungseok Seo and Dongik Lee. Determining the length of static message for efficient use of flexray network. *SICE Annual Conference 2010, Proceedings of*, pages 563 –566, aug. 2010.

[13] Haibo Zeng, M. Di Natale, A. Ghosal, and A. Sangiovanni-Vincentelli. Schedule optimization of time-triggered systems communicating over the flexray static segment. *Industrial Informatics, IEEE Transactions on*, 7(1):1 –17, 2011.

The Possibility of Wireless Sensor Networks for Commercial Vehicle Load Monitoring

Jieun Jung*, Byunghun Song
RFID/USN Convergence Center
Korea Electronics Technology Institute
Gyeonggi-do, Republic of Korea
{jejung, bhsong}@keti.re.kr

Sooyeol Park
IT Convergence Research Center
Innosensing Corporation
Seoul, Republic of Korea
cto@innosensing.co.kr

***Abstract*—It is of great importance to be able to monitor and enforce vehicle weight limits for road authorities involved in almost all aspects of transportation and pavement engineering. For the active control of additional weight carried by overloaded vehicles, essential IT technologies such as sensors, measurement, and data processing have been applied. The integration of vehicle load monitoring systems with Wireless Sensor Networks (WSN) technology has a possibility of reducing installation efforts and costs, and enabling the quick and easy configuration of data acquisition and control systems. In this paper, we try to verify that WSN technology can replace the wiring sensor applications for vehicle monitoring issues. The WSN-based system includes: inclinometer sensors which measure variation of inclination values with load changes;, an Access Point (AP) that logs the data collected from all these sensors;, and a weight estimation algorithm. To reach the goal, we performed an experiment with real deployment and estimated the weight of trucks with an error of less than 3%. The result shows that it is possible to adopt WSN for commercial vehicle load monitoring.**

Keywords-component; vehicle, inclinometer, WSN, weight estimation, inclinometer sensor

I. INTRODUCTION

Recently telematic technologies used for vehicle information have provided a number of practical services, such as vehicle/traffic tracking, vehicle/road safety, and entertainment services. [1] To start with, vehicle/traffic tracking services are already deployed on a commercial scale, and drivers on the move can be informed of their location, movement, and status in real-time by using mobile systems such as navigation systems, cell phones and so on. Furthermore, electromechanical sensors embedded in vehicles, such as pressure, acceleration, and temperature sensors help drivers to maintain the safety of surrounding vehicles.

However, vehicle accidents on the road have been on the increase, especially accidents caused by huge commercial vehicles including trucks and, trailers, and these are becoming a big issue nowadays. According to an analysis of traffic accidents in the Republic of Korea in 2008, 4.7 % of vehicle accidents were caused by huge commercial vehicles, but they caused 12.5% of death from traffic accidents. This reveals that accidents involving huge commercial vehicles are more likely to cause severe results. [2]

With the development of the distribution industry, more active control of overloading vehicles also becomes necessary for the management of highways and bridges. Overloading is one of the biggest elements which have a great influence on the deterioration of this SOC (Social Overhead Capital). When vehicles containing dangerous chemicals or fire risk materials overturn, this can even bring unexpected aftereffects. Hence, it is of great importance for the maintenance and operation of the road and bridge infrastructure to monitor and prevent vehicle overloading. Vehicle information, which is the basis of the successful creation of safety traffic environments, should be both collected and analyzed.

Various studies on monitoring over-weight vehicles have shown the benefits of monitoring them. At present, all road authorities use either stationary vehicle scales along the route or Weight-In-Motion (WIM) systems at toll plazas for vehicle load enforcement, although it involves expensive installation and calibration procedures. Firstly, static weight stations are inefficient in that they force vehicles to enter the stations and wait for the process in a queue. [3] To resolve this problem, mobile weighing systems have also been introduced and installed everywhere with no limitations. However, there still require vehicles on the move to stop.

Lastly, WIM systems are designed to capture and record vehicle axle weights and gross vehicle weights when they drive over in-pavement sensors such as road cells. Unlike the above static weight stations, they do not require the subject vehicle travelling in traffic lanes to stop. However, it is still challenging to calculate weight accurately without any vehicle information such as fuel type, year, model and so on. Furthermore, WIM systems are highly sensitive to electromagnetic disturbances caused mostly by lightning strikes in the vicinity of the equipment. [4, 5]

In a different approach, weighing systems embedded in the vehicles have also been designed. [6] However, the weighing systems implemented using wired communication methods have difficulties in wiring and configuration constraints. Vehicles such as cargo trucks also have trouble disassembling part of their system because they fold their back trailers in case they are empty. Therefore, we surveyed

wireless technology and found that WSN technology could be an advance in commercial vehicle overload monitoring. WSN based on inclination measurement was designed, calibrated, and tested to examine the possibility of using WSN for commercial vehicle load monitoring.

To fulfill the requirements, we first designed a WSN-based inclinometer sensor that measured inclination values with variations of load changes. The sensor has many unique challenges: the sensor needs to be insensitive to the other sensors and nearby electrical equipment and should have a long lifetime; the sensor has to be resistant to water and temperature; and a package of sensor nodes should be designed to simply be attached and removed from the vehicles' suspensions.

Given inclination measurements from the wireless inclinometer sensors, we still need to construct a load estimation algorithm that has good performance. There is an important challenge in estimating the weight of vehicles: the values of inclinometer sensors are greatly affected when they are used in lanes on slopes or rocky roads. In this paper, we introduce an approach that handles the challenge by utilizing both reference sensors and sensors to measure changes of tandem axles. To evaluate the performance, experiments which targeted 34 to 43 ton trucks were performed in a real environment. Moreover, we estimated the weight of the trucks with an error of less than 3%.

This paper is structured as follows: In Section 2, we present the specific design and rationale of the proposed a vehicle load monitoring system based on WSN. Section 3 examines the possibility of using WSN for commercial vehicle load monitoring with real implementation. Section 4 concludes the paper

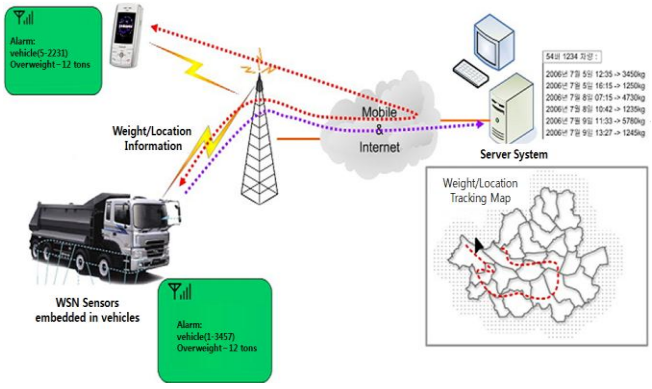

Figure 1. Semantic Diagram of WSN-based Vehicle Load Monitoring System Layout

II. WSN-BASED VEHICLE LOAD MONITORING SYSTEM

In this section, we propose a WSN-based commercial vehicle load monitoring system to solve the problem and we detail the main challenges that need to be addressed. Our main approach to monitoring the load of vehicles is to use WSN-based inclinometer sensors which estimate vehicle load changes with variations of inclination values. The proposed system shown in Fig 1 consists of three main components: inclinometer sensors attachable to suspensions, and an Access Point (AP), and a weight estimation algorithm.

The following section presents how we developed and implemented the sensor design of the wireless inclinometer sensors, including the choice of inclinometer, casing and noise filters. We then describe the transmission protocol developed for this sensor node and the weight estimation algorithm in detail.

A. Sensor Node Design

TABLE I. INCLINOMETER DATA (SCA-61T-FAHH1G)

Parameter (units)	Performance characteristic
Sensitivity (V / g)	4
Noise Density (° / Hz)	0.0008
Current Consumption(mA)	2.4 ~ 4
Min. Operating Voltage(V)	4.75

We selected a MEMS (Micro Electro Mechanical Systems)-based single axis inclinometer, SCA-61T-FAHH1G, made by VTI Technologies, due to its low temperature dependency, high resolution, and low noise. [7] The SCA-61T-FAHH1G measures ranges of ±30° and with a resolution of 0.0025° (10 Hz BW, analog output) and other data about the inclinometer are shown in detail in Table 1. We then built an inclinometer sensor node using a small IC chip in which detection, signaling processing algorithms, and data transmission modules coexist as built-in-units. The sensor node is loaded with a low-power inclination measuring device, a microprocessor, and an RF transmitter and call signals. Data acquisition and all processes are performed by the sensor node itself. The microprocessor controls all the functions, including signal measurements, and executes the analysis algorithm. The measured inclination signal outputs and analyzed results are transmitted to a remote server through an RF transmission module, Zigbee PHY(CC2420). The device measures inclination in the given frequency ranges from inclinometer sensors in real time.

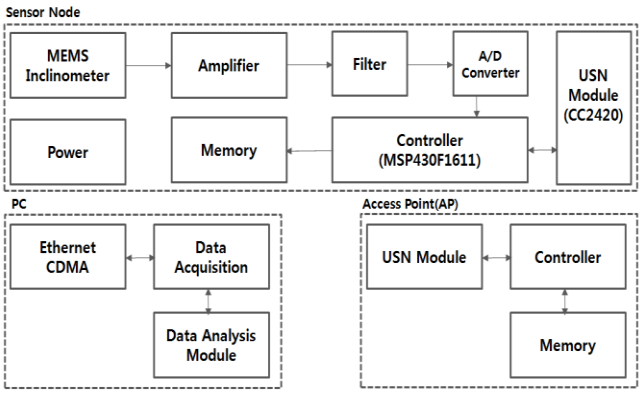

Figure 2. Block Diagram of the Inclinometer Sensor Node/AP/PC

TI MSP430 is used as the main processor, and the RF transceiver consists of a four-wire SPI interface. Monitoring of the data and movement of each platform is done via RS-232 communication. The interface is made for JTAG (Joint Test Action Group) and SPI (Serial Peripheral Interface), are used for programming the board. An MFC interface is used with a two-pin connector, which is designed to act as an A/D transformation port and execute GPIO (General Purpose Input/output) through an ATmega128 setting so that the MFC interface can be used as an all-purpose interface. The Silicon Serial Number IC used for the ID of each board reads data only through a 1-wire interface. [8] Figure 2 shows a block diagram of the electronic circuit of the WSN-based inclinometer sensor node.

B. Transmision Protocol Design

For wireless transmission, we adapted the Zigbee and the architecture of the protocol consists of wireless sensor nodes, bridges and the AP. At the physical layer, the AP and all the nodes use an IEEE 802.15.4 compatible radio transceiver which uses the 2.4 GHz ISM band at a data transmission rate of 250 Kbits/s. The AP has both a wired and a wireless connection. The wireless connection is used to communicate with the sensor nodes while the wired connection of the AP is used to communicate with the PCs.

The MAC (Medium Access Control) layer is based on the TDMA for its reliable data transmission. The inclination data is transmitted in a series of rounds, and each round has a fixed number of packets to transfer, called the window size. For example if we have 100 packets and a window size of 5, the 100 packets are divided into 20 rounds. Only one acknowledgment is transmitted back to the sender, and lost packets in each round are retransmitted by looking at the lost packet information in the acknowledgment. Once the receiver has acquired every packet in the current round, the sender and receiver can move on to the next round. This prevents any packet collisions in the networks.

Moreover, we used a specific parameter, RF Group ID, to avoid radio frequency interference from surrounding wireless devices or systems. When data packet is transmitted, the AP will check whether it contain the same group id or not .

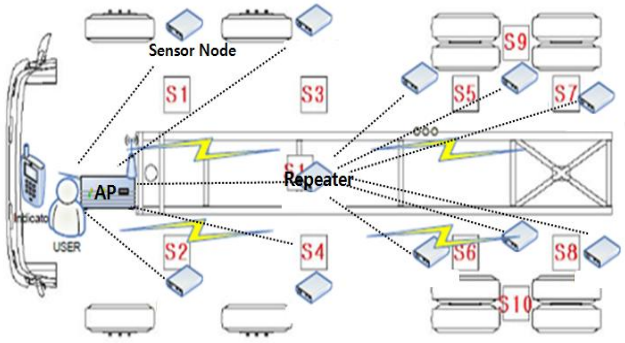

Figure 3. Communication architecture of protocol in vehicles

The transmission protocol is designed to meet both the reliable communication and power efficiency requirements. All sensor nodes can reach AP or repeater (if necessary) in one hop, and the AP with unlimited power supply can communicate with the sensor nodes in one hop. The simple architecture of this protocol is shown in Figure 3. We agreed that the exclusion of multi-hop transmission between sensor nodes can limit the network coverage by the maximum transmission range between the AP and repeater nodes. However, this network coverage is sufficient for our implementation of the vehicle load monitoring system.

We here adapted the low power listening algorithm which repeats sleep and wake period to save power consumption of sensor nodes. It enables them to stay awake for the minimum amount of time and prevent packet collisions. The procedure of our transmission protocol can be described as follows:

i. All the sensor nodes are configured with pre-assigned radio channel and a transmission time slot before installation.
ii. The AP sends a periodic synchronization message to the sensor nodes.
iii. The radio of all the synchronized sensor nodes will wake up and check if there is any transmission during its time slot, and go back to sleep if there is none.
iv. After completing data acquisition and processing, the AP transmits vehicle load information to its main server or navigation according to its data type .

C. Weight Estimation Algorithm

To accurately estimate the weight of vehicles, we designed a weight estimation algorithm based on the inclination measurements. We also improved the algorithm by using reference sensor nodes to correct the error of the slopes. The main principle of this algorithm is that the load of the vehicle is directly affected by the suspension which is a system of springs, shock absorbers, and linkages connecting a vehicle to its wheels. In other words, there is a correlation between changes of inclination and the vehicle-weight before and after loading. [9] Firstly, we dealt with the spring type suspensions generally installed in commercial vehicles.

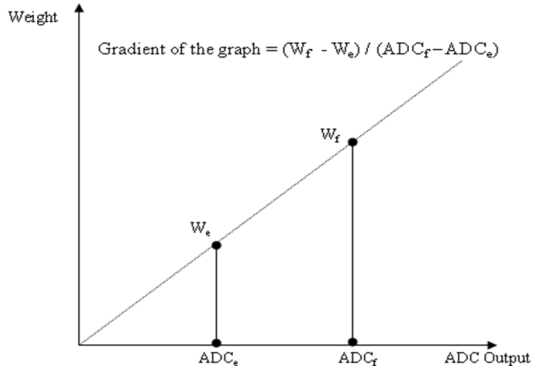

Figure 4. Example of Estimating Weight Graph

Given the ADC value of sensor output S_{ADC}, weight of the empty W_e and full vehicle W_f,, there exists a linear relationship between the ADC value and weight. Figure 4 shows an example of an estimating weight graph and Factor, the gradient of this graph, is $(W_f - W_e) / (ADC_f - ADC_e)$. The expected weight of the vehicle W_{ex} can be calculated by following equation (1).

$$W_{ex} = \text{Variation of } S_{ADC} \times \text{Factor} + W_e \quad (1)$$

However, this algorithm may produce incorrect results when vehicles are used in lanes on the slopes or on rocky roads. To develop an adjusted estimation algorithm, a reference sensor S_{1st} measures the inclination of the road and a sensor S_{2nd} to measure changes of a tandem axle are additionally adopted. The expected weight of the vehicle W_{ex} for independent wheel suspension and tandem suspension can be calculated using the following equation (2).

$$W_{ex} = (\text{Variation of } S_{ADC} \pm (S_{1st\_ADC} \text{ or } S_{2nd\_ADC})) \times \text{Factor} + W_e \quad (2)$$

Based on an analysis of the accuracy in the experiment, we also found that duplication sensors S_d attached at both ends of an independent wheel suspension are necessary to estimate more accurate results. It often happens that the left and right sides of the suspension show different variations when they move on slopes. In this case, Factor, the gradient of this graph, is $(W_f - W_e)$ / (Average Variation of S_{ADC} ± variation of $S_{1st\ ADC}$). The expected weight of the vehicle W_{ex} can be calculated using the following equation (3).

$$W_{ex} = (\text{Average Variation of } S_{ADC} \pm S_{1st\_ADC}) \times \text{Factor} + W_e \quad (3)$$

III. EVALUATION

In this section, we evaluated the performance of the proposed WSN monitoring system and Weight Estimation Algorithm at the test bed site. For the experiment, we installed inclinometer sensor nodes and APs in a real deployment, and chose three geographical features such as flat and rocky roads and slopes. Section A explains how we reduced the noise of the inclinometer sensor, Section B compares the performance of basic Weight Estimation Algorithm and the adjusted Weight Estimation Algorithm with additional reference and duplication sensors.

A. *Inclinometer Sensor Performamce*

We measured the noise of the installed inclinometer sensor 1000 times at 100ms interval with no environmental interference (repeated 3 times). At first, the ripple measured was almost 4 ~ 5°, as shown in Table 2, since the power is not uniformly supplied. To reduce the supply noise, we applied a Regulator, LC filter, and LDO (Low Drop Output) and it shows the best result with 0.105° when both the LC filter and the LDO are adopted as shown in Table 3. However, the software should be supported for further improvement.

TABLE II. SENSOR OUTPUT WITHOUT LDO, LC FLTER

	Min	Max	Ripple	Avg	Median	Mode	Var	St. Dev
1	-2.624	1.364	3.988	-0.655	-0.655	-0.909	0.394	0.628
2	-2.729	1.574	4.303	-0.632	-0.665	-0.944	0.413	0.643
3	-2.834	2.414	5.248	-0.590	-0.595	-0.665	0.533	0.730

TABLE III. SENSOR OUTPUT AFTER APPLYING LDO, LC FLTER

	Min	Max	Ripple	Avg	Median	Mode	Var	St. Dev
1	1.084	1.189	0.105	1.128	1.119	1.,.119	0.000	0.017
2	1.084	1.189	0.105	1.131	1.119	1.119	0.000	0.020
3	1.119	1.224	0.105	1.154	1.154	1.154	0.000	0.021

B. *Estimation Algorithm Performance*

1) *Experimental Setups*

We targeted 4 different trucks from 37 to 47 tons, as shown in Figure 5, and deployed inclinometer sensor nodes (ch 1 ~ ch15) and APs as presented in Figure 5. In Figure 5, ch 15 is an overall reference sensor, and ch 13 and ch 14 are tandem reference sensors. The experiment was repeated 80 times for each geographical feature; flat, rocky roads, and slopes, and the average value of the weight was used. The error is defined to be the difference between the weight measured by scales and the weight estimated by the basic and adjusted algorithms.

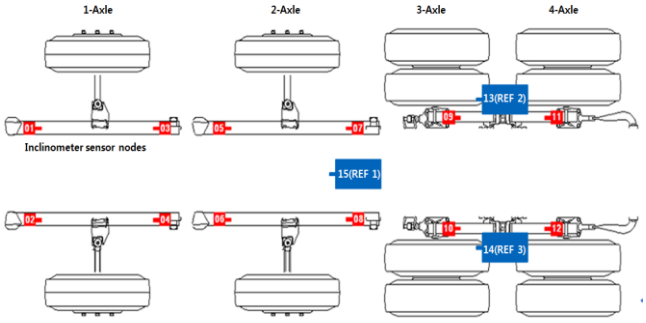

Figure 5. Experimental Setups

2) *Result Data Analysis*

We applied the basic Weight Estimation Algorithm and the adjusted algorithm using reference and duplication sensors. Table 4 summarizes the performance of the two algorithms for each geographical feature. In the case of the flat road, the two algorithms show almost the same error rate, from + 1.5% to - 1.6 %. In the case of the slopes, we conducted the experiment on both uphill and downhill roads. The error rates of the uphill and downhill road were similar, ranging from + 3.5% to - 1.4 %, and the error rate was decreased by approximately 0.3% when the adjusted algorithm with the reference sensors was applied.

Finally, in the case of the rocky roads, the error rate was from + 2.5% to - 2.0 %, and the error rate was decreased by approximately 0.3% when the adjusted algorithm with the reference and duplication sensors were applied. Through this experiment, we found that the adjusted algorithm improves the performance of the weight estimation by 0.3%, but it is still challenging to find right location and to install the additional sensors.

TABLE IV. PERFORMACE OF WEIGHT ESTIMATION ALGORITHM (%)

	Flat road		Slope				Rocky road	
			uphill		downhill			
	min	max	min	max	min	max	min	max
WEA	-1.6	+1.5	-2.4	+2.5	-0.8	+5.6	-2.0	+2.5
Adjusted WEA	-1.6	+1.6	-0.5	+4.2	-1.3	+4.5	-1.3	+2.9

C. Commnincation Perfomance

An experiment was carried out in order to evaluate the impact of the driving vehicle speed and vibration on the sensor node's measurements. We measured inclinometer data while the vehicle is on the move at normal speed (70 to 100km/h). The Figure 6 and Figure 7 represent the result when the vehicle moves and stops representatively. Based on the result, we confirm that all the sensor data is transmitted to the AP without loss. Only variation of magnitude is relatively high when the vehicle is moving.

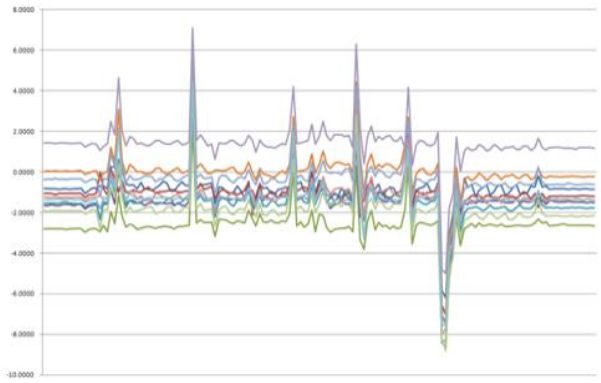

Figure 6. Inclinometer data when the vehicle stops

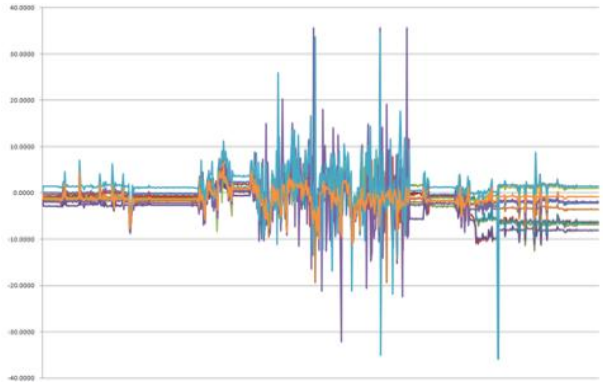

Figure 7. Inclinometer data when the vehicle is on the move

IV. CONCLUSION

In this paper, we verified that WSN technology can be applied to existing wired sensor applications in heavy vehicle load monitoring. To reach the goal, we proposed a vehicle load monitoring system based on WSN, and presented experimental results obtained in real environments. Our main approach to monitoring the load of vehicles is to use WSN-based inclinometer sensors which estimate vehicle load changes with variation of inclination values. From the experiment, we also confirmed that the weight of the reference vehicles was estimated with an error of less than 3 %. This result shows that it is possible to adopt WSN for vehicle monitoring.

However, we also found that simultaneous transmission over the various channels still remains a challenge because the amount of data was larger than the maximum channel capacity. And the number of sensors deployed in the vehicle should be minimized. To figure out this issue, additional research and experiments in real environments should be conducted to guarantee a future reliable and reasonable monitoring system based on WSN.

ACKNOWLEDGMENT

This work is supported by the IT R&D program of MKE/KEIT (No. 2010-10038668) and by a grant (10CCTI-A052535-03-000000) from the Ministry of Land, Transport and Maritime of Korean government through the Core Research Institute at Seoul National University for Core Engineering Technology Development for Super Long Span Bridge R&D Center.

REFERENCES

[1] Roy C. Hsu., and L. R. Chen, "An Integrated Embedded System Architecture for In-Vehicle Telematics and Information System", Proc. IEEE ISIE 2005, pp. 1409–1414, June 2005

[2] Simon Jeong, "An Analytical Study of Heavy Weight Trucks' Traffic Accidents and Countermeasures:: on the Gyeong-bu Expressway", Master thesis, 2007

[3] Kwon Soonmin, Park Heuigu, Kim Jiwon, Kang Kyoungkoo, and Lee Dongjun, 17th ITS World Congress Busan, October 2010

[4] Qiu sheng Ru, Yang Yang, Zong qi Ning, Tao Song, " The Application of Nerve Net Algorithm to reduce Vehicle Weight in Motion System Error", International Conference on Optoelectronics and Image Processing, vol. 2, pp. 511-514, November 2010

[5] Teerachai Deesomsuk, Tospol Pinkaew, "Evaluation of effectiveness of vehicle weight estimations using bridge weight-in-motion", The IES Journal Part A: Civil & Structural Engineering, vol. 3, pp. 96 – 110, 2010

[6] Xiaohau Jian, Shhram H. Vaziri, Carl Haas, Leo Rothenburg, Gerhard Kennepohl, Ralph Hass, "Improvements in Piezoelectric Sensors and WIM Data Collection Technology", Auunal Conference & Exhibition of Transport Association of Canada, 2009

[7] http://www.vti.fi/midcom-serveattachmentguid-2b9fadebe6fa4a0c24f144cd55fda22d/SCA61T_inclinometer_datasheet_8261900A.pdf

[8] Sukwon choi, Jieun Jung, Byunghun Song, and Sooyel Park, “Possibility of Wireless Sensor Networks for Outside Exposed Gas Pipeline Monitoring”, International Conference on Information Processing in Sensor Networks(IPSN) RealWIN Workshop, 2011

[9] Nicola Amati, Andrea Festini, Luigi Pelizza, Andrea Tonoli, “Dynamic modeling and experimental validation of three wheeled titling vehicles”, International Journal of Vehicle Mechanics and Mobility Special Issue, vol. 49, 2011

Real-time routing for low-latency 802.15.4 control networks

Koen Holtman, Peter van der Stok
Philips Research, Eindhoven
High Tech Campus 34, 5656AE Eindhoven, the Netherlands
{koen.holtman, peter.van.der.stok}@philips.com

Abstract

In many applications of wireless control networks, the latency of message delivery is an important consideration. In a lighting control network where a light switch sends a wireless message to a lamp, a worst case end-to-end latency of 200 ms or better is desired, so that the working of the switch feels 'immediate' to the end user. This paper studies the probability that latency deadlines of a few hundred ms are exceeded. We use a 802.15.4 test network, located in a real-life office environment, to evaluate and compare the effects of several re-try and re-routing strategies. Testing under realistic conditions, in an office environment when people are present, is important to accurately determine worst case latency performance as experienced by end users. At night, without any people in the building, performance is much better than during the day. In order to accurately observe the effect of different strategies, test runs lasting at least a week are needed. We find that retrying message delivery via a single delivery route is sub-optimal. Keeping a set of two or more candidate routes for subsequent re-tries greatly improves worst-case latency.

1 Introduction

A wireless control network differs from the more commonly considered wireless sensor network (WSN) because it incorporates actuators in addition to sensors. Whereas in most WSN designs, the object is to get all sensing data forwarded to a central (logging) location for later analysis, in a wireless control network the object is to control actuators based on data from close-by sensors. Home and office control systems are important applications of wireless control networks. The low cost of wireless sensor nodes, and their ability to run on batteries, makes it feasible to equip rooms with many sensors, which can be used to increase both comfort and energy efficiency.

The reliability and latency of a wireless building control system must be just as good as that of the wired system that it replaces. Consider the case where a lamp in a room is wirelessly connected to a switch on the wall. In such a setup, it is not the average end-to-end latency that will be important for the quality perception of the user, but the worst-case latency. If the latency is too high too often, the system will break the 'immediacy' mental model that the user has for light switches, which negatively impacts the user experience and ultimately the user acceptance. Our design goal is to minimize the probability that 200 ms latency is exceeded. As a rule of thumb in user interface design, 200 ms latency is still short enough that the user can accept the relation between stimulus and response as 'immediate'.

Contrary to most publications we are less concerned with the maximum achievable throughput, average-case latency, or scalability of the routing algorithm. We expect that most communications in building control will not need more than 2 hops, with 4 hops being exceptional. We therefore focus on quality improvement of the 1-hop and 2-hop cases, which represent the bulk of the wireless control communication in the building.

We concentrate on the effects of multipath fading which lead to unexpected link failures of very good links during the day time. Effects coming from interference caused by the high density of nodes are not investigated. Therefore, the measurements concentrate on a relatively low number of nodes reflecting the node and message density we expect for building control

2 Measurements in literature

This paper is motivated by measured communication behaviour in buildings with occupants. In the literature measurements on wireless communication have been done to measure: Point to point communication, Sharing the medium between multiple senders, and Routing over a large dynamic network. This section summarizes the main published results as introduction to our routing suggestions to improve the probability that packets arrive in time (within their deadline).

A naïve model of transmission by an omni-directional antenna in empty space, states that the strength of the signal decreases with the square of the distance [9]. Unfortunately, space is not empty but is populated with reflectors and absorbers of the RF signal. Reflections from surfaces can meet the original signal with a slightly different phase thus reducing or completely removing the signal. Report [9] shows that most simple propagation models used in simulations do not correctly represent the transmission as measured in situ. Measurements of the communication quality between a single sender and a receiver indicate that there are usually three regions: (1) a clear region with little or no reception losses, (2) a transitional region where packet loss ranges from a few percent to complete loss unrelated to the transmission distance, and (3) a region where almost no packets are received.

Over time the link quality fluctuates as well. These phenomena are reported in [1][2]. The clear region for IEEE 802.15.4 [3] is reported to be on average between 3 and 15 meters in [5][6][8], where in some cases the signal had

to penetrate office walls. In [7] it is observed that the height of the sender has a significant impact on packet yield. Papers [1], [4], [5] and [7] show that RSSI is not a good indicator for success rate. Link quality Indicator (LQI) is seen to perform better in [7]. From the papers we learn that the transmission range depends on the direction, that channels are not necessarily symmetric, and that channel strengths change over time, and height of node. Assuming that the point to point transmission is in the clear region, dependent on the load and the number of load generating senders, the medium throughput around a given node still suffers from multi-sender interference. In [4], confirmed by [6] it shown that the total throughput obtained with one sender is divided by two when four senders try to occupy the channel. The lowered throughput can come from the many retries, the larger back-off times associated with retries, or the loss of packets.

The behaviour of the links over time is discussed in [10]. Conclusions are that the number of packets needed for successful transmission is a better quality indication than Reception Rate (RR). Another conclusion is that at a given time the stable link is the best link to use and that failure over a stable link is accompanied by failures over the unreliable links as well. In [2] and [12] it is shown that link quality and not hop count should be at the basis of link selection. In [12] also the unpredictable stability over the day is shown. In contrast to earlier papers, the measurements in [13] suggest that RSSI is a good indicator of link quality. The authors conclude that the new chip technology of the CC2420 improved the usability of the RSSI value. In [14] it is shown that irregularity of the radio signal has a high impact on the routing efficiency. In [11] and [13] an overview of wireless communication link-failure over time is presented.

The notion of real-time deadline and delay is not frequently cited in the context of routing. The authors of [15] show that no guarantees on end-to-end delays can be given but that we are confronted with an end-to-end delay probability distribution. This notion has led to the development of the SPEED protocol where the probability of meeting a deadline was recalculated during the progress of the packet over the multi-hop path [16]. The SWR protocol [17] uses multiple paths routing while removing packets which will not meet their deadline. Another probabilistic real-time routing protocol is presented in [18], where the forwarding time is estimated for each hop during transmission.

In this paper we investigate link performance over at least a week and try different routing and packet retry schemes to improve the transmission success rate within the deadline. This paper extends existing work by:

- Observations over periods of at least a week,
- Testing links that are in the clear region,
- Observation in an office building during working hours,
- Concentrating on one-hop and two-hop routes.

3 Test network

Building on our earlier work [19][21], we constructed a test network with 8 network nodes in an office building, and did extensive measurements on latency. Walls are made of plasterboard, but the offices contain many large metal filing cabinets, creating a strong multi-path environment. Node locations for the tests are shown in figure 1. Each node 1-7 is a sensor node, sending messages with (arbitrary) sensing data to node 0, at random times with an average rate of 2.7 messages per second per sensor node. This high message rate is too high for a control network in real-life situations, but it does ensure that we can gather sufficient statistics in a test run lasting about a week. As shown in figure 1, the nodes 0-4 are all in the same office. We located them behind obstacles in this office in such a way that there is no direct line of sight between them – this means that multipath cancellation (Rician or Rayleigh fading) can cause link failure even inside this office.

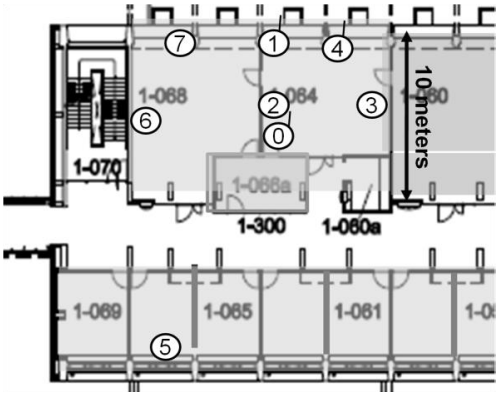

Figure 1, Sensor nodes 1-7 send messages to node 0.

The nodes use the 802.15.4 protocol in the 2.4 Ghz band, and are implemented using Jennic JN5139-Z01-M00/M001 wireless modules [20] with custom software implementing the delivery algorithm in figure 2. Nodes 0,1, and 4 have whip antennas, the other nodes have small ceramic antennas. All nodes can communicate directly with node 0, although the link quality between node 5 and node 0 proved to be lower than between the other nodes and node 0.

The messages are fixed-length and very small. Including protocol overheads, an 802.15.4 packet carrying a message has a length of 27 bytes. We use the 802.15.4 MAC unicast mechanism with acknowledgments, so that each node does 4 packet sending re-tries whenever it finds a clear channel. In an outer loop, the MAC is invoked every WT milliseconds until an end-to-end acknowledge message (sent by node 0 via the reverse route) is received. WT is a parameter which is set to 40 ms in most of the measurements.

Routes can contain multiple hops. If a node receives a message that it should forward, according to the routing instructions in the message, the node will invoke IEEE_802.15.4_MAC_unicast_with_ack() once to do the forwarding. If this fails, the routing node will discard the

message. The original node will do a retry, possibly via another router, when its timer t2 runs out.

```
deliver_message(m) {
    start timer t1 counting up from 0 ms;
 do {
    pick a delivery route r;
    format message m with route r into packet p;
    start timer t2 counting down from WT ms;
    IEEE_802.15.4_MAC_unicast_with_ack(p);
    wait_until( (t2 < 0) ||
        (end-to-endacknowledgement received from MAC) );
 } while(no end-to-end acknowledgement received)
   measured_message_latency = t1;}

IEEE_802.15.4_MAC_unicast_with_ack(p) {
 Try to detect a clear channel, with exponential backoff;
   // we use MaxCSMABackoffs=4 and minBE=1 so this
   // phase takes between 1 and 19 ms.
 if(no clear channel found) return;
 for(i=0; i<4; i++) {
   use radio to send packet p; // takes ~2 ms
   use radio to listen for MAC acknowledgement
    packet; // takes ~1 ms
   if(valid MAC acknowledgement packet heard) break;
 } }
```

Figure 2 Message delivery algorithm used by nodes.

Several variants on the algorithm in figure 2 are possible. For example, if the MAC fails to deliver a message with acknowledgment, the outer loop might retry immediately, rather than waiting for t2 to run out. We have not (yet) tested this variant – it creates a larger risk of packet storms in the system, but the speedup might be worth-while.

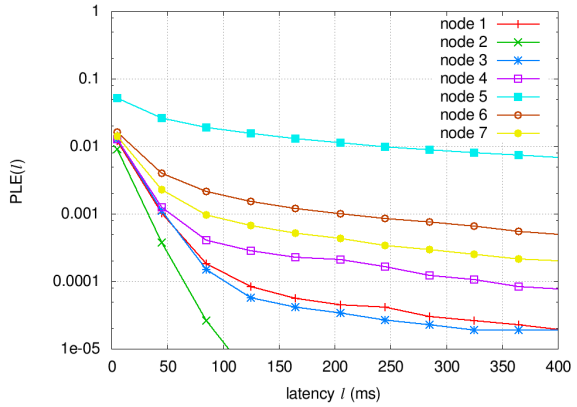

Figure 3 PLE(*l*) for all nodes with 1-hop route to node 0.

4 Single hop latency

We consider the latency of routing along a single hop: we do a test where all sensor nodes always choose the direct route to node 0 to deliver their message with WT=40 ms. In order to get sufficient statistics about the infrequent high latencies, we run the test network for many days. This creates test logs containing millions of message latency measurements per node. To interpret the test run data, with a focus on the question of how the end user will experience the latency, we found it instructive to define the metric PLE(*l*): the probability that a latency *l* is exceeded by a message. We compute it as follows from a test run:

PLE(*l*) for node *n* =

(number of messages sent during office hours by node *n* with measured_message_latency >=*l*) / (total number of messages sent during office hours by node *n*).

Because of our interest in human-observable latency, the PLE calculation does not consider messages sent outside of office hours – this is discussed in more detail in [19]. Figure 3 plots PLE(*l*) for all sensor nodes, showing large differences for the nodes. Node 2, closest to node 0, has the best (lowest) curve. Node 5, furthest from node 0, has the worst. For the other nodes, there is no strong correlation between curve position and the distance of the node *n* to node 0.

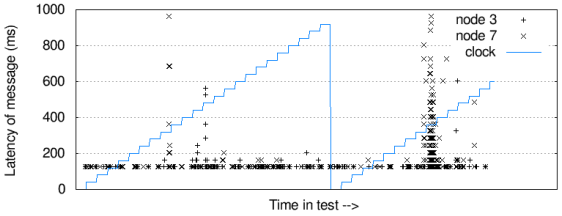

Figure 4 Messages with latency higher than 125 ms.

Figure 4 shows how high latencies occur over time, for nodes 3 and 7. The X axis is time over 38 hour section of run taken for figure 3, the saw-tooth line plots a 24-hour clock. The high latencies occur almost exclusively during office hours. Node 7 experienced latencies higher than 1000 ms off the Y axis scale. We see that a node can have 'good days' where a given latency deadline is never, or almost never, exceeded, and 'bad days' where it is exceeded often within a few hours. Test runs have to be long because every node needs to have a chance to experience its 'bad days' at the rate that they happen for that node. The unpredictability of the number of 'bad days' in a week, and the possibility of long term changes in the environment, makes us cautious in comparing curves from different test runs. To measure the differences between alternative message delivery strategies, we use a single long test run in which the nodes switch to a random different strategy every 10 minutes. Our testing approach extends earlier work, where conclusions were drawn on the basis of shorter run durations under cleaner conditions.

5 MAC invocation interval WT

With WT=40 ms, a failing link makes the node invoke the MAC, every 40 ms, sending at most 4 packets. So if a link is failing, WT=40 ms generally leads to a PHY packet sending rate of 100 packets per second, until success. This is an excessively high rate which may lead to packet storms. In [21], we used a 5-node test-bed to investigate the effect of varying WT. Some indicative results from [21] are shown in figure 5. Node 4 in the test bed used was far away from node 0, for this node we see an im-

provement when lowering WT. This is conform expectation, because the time between retries is smaller and consequently the probability of meeting the deadline for a given number of retries is higher.

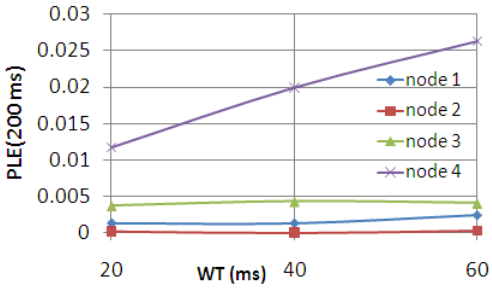

Figure 5 Effect of WT on PLE(200ms) for 4 nodes on different test bed, with 1-hop routing to node 0.

However, for the other nodes, closer to node 0, we see no difference that is statistically significant for a one-week test run. Apparently, with values of 66, 100, and 200 PHY packets per second, we are well past the point of increasing returns for these short hops. This can be explained as follows. First, if a link suffers from significant path fading for a duration much larger than the packet size, sending packets faster will not help. Second, the positive effect of sending more packets might be counterbalanced by the negative effects of longer medium occupation. Third, while the MAC is waiting for a clear channel, its 802.15.4 radio will not be able to receive an end-to-end acknowledge message directed to it. Instead, the MAC will interpret the attempt to deliver the message as a busy channel, causing it to wait. Finding out which of these effects, if any, is dominant needs more study.

In a similar test run on the 8-node test-bed of figure 1, we again saw no significant difference, for PLE(l) with l>100 ms, between WT=20 and WT=40. For all test results in this paper we therefore use WT=40 ms.

6 Improvement by adding more candidate routes

Except for nodes 5 and 6, the curves in figure 3 are satisfactory, from the standpoint of human-observable latency. Nevertheless, an optimization that makes the curves go down more steeply, increases the quality of the user experience. As we discussed more extensively in [19], a lot of the high latencies in figure 3 can be attributed to multipath fading of the single link. Performance can be improved if the sensor node maintains a list of multiple candidate routes, and re-tries along other routes if attempts along the preferred route fail. Figure 6 shows the performance of the test network with an improved routing scheme. Each node first tries the direct route to node 0 twice. If that does not work, routing via node 1 is tried, and if that does not work routing via node 2. If that still fails, the direct route is tried twice again, and so on. Values of PLE(200 ms) are greatly improved (reduced) except for node 2, which goes from extremely good to merely good.

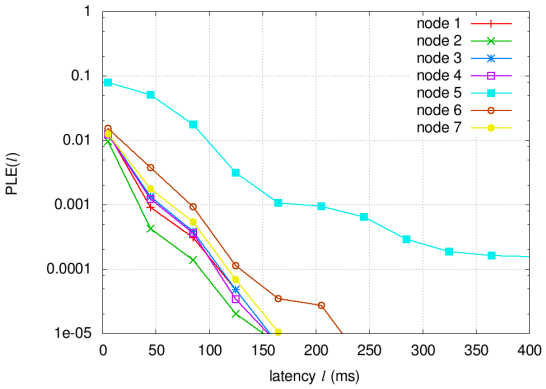

Figure 6 PLE(l) for all nodes using 3 candidate routes.

7 Two-hop latency

We now turn to the study of two-hop routes. We measure the PLE for message delivery along each of the all possible 1-hop and 2-hop routes to node 0. In this test run we decrease the message sending rate in the system to 1.4 messages per node per second, to avoid a situation where system self-interference becomes a dominant factor in determining PLE. Each route is tested individually: the node keeps trying the route under test until the message is delivered. Over the course of 2 working days, each route was tested by sending 12500 messages over it on average. This number was sufficient to determine PLE(l) up to l=165 ms with reasonable statistical accuracy. A longer test run might show a different picture with PLE scores that are sometimes lower, because nodes have a bigger chance of experiencing a 'bad day'.

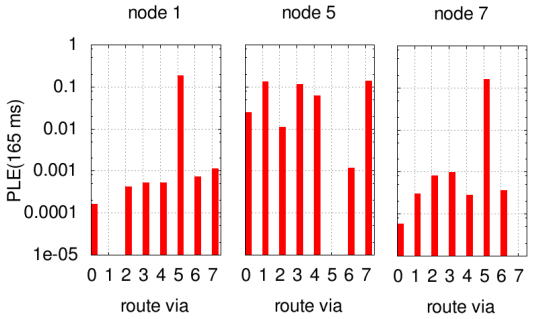

Figure 7 PLE(165 ms) for all 1-hop and 2-hop routes starting at nodes 1, 5 and 7.

Figure 7 shows some representative measurement results. As in figure 3, we see a spread in route quality. For all nodes but node 5, the 1-hop route directly to node 0 (the bar labelled 0 in the graphs) out-performs all 2-hop routes by a significant margin.

8 RSSI usage

As it takes a long time to measure PLE curves accurately, an obvious question is whether PLE could be predicted based on RSSI given the contradictory results from the literature presented in section 2. In the same test run we also measured the average RSSI value of each link. Also

we devised a measure to combine the RSSI values of the two links involved in a two hop path (called the route RSSI). In figure 8 we plot the relation between PLE(165 ms) and the route RSSI. The route RSSI for a 2-hop route is computed by multiplying the RSSI values of the two hops. We also tried addition and taking the minimum, but found that multiplication gave the best result in terms of PLE correlation. Looking at the 2-hop routes only, we see that a very low RSSI, RSSI <20, is a good predictor for a bad route. For RSSI>20 however, there is no longer any visible correlation between RSSI and route quality. Apparently, in this region, the link budget along the route is so high that, with the number of retries we do, it stops being the dominant mechanism in determining PLE. Therefore, if we are to find the best 2-hop routes with a high probability, we have to measure their actual PLE, though an RSSI cut-off at 20 can be used to reduce the number of routes to be measured.

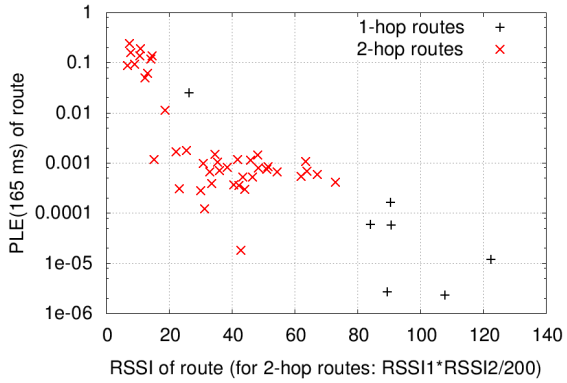

Figure 8 PLE(165 ms*)* versus route RSSI in test network.

Another technique to save resources in selecting routes is to base selection on PLE(*l*) measurements with *l*<165 ms, which can be measured more quickly. We have observed that the PLE curves hardly cross in the region from 85 to 165. Therefore using PLE(85 ms) instead of PLE(165 ms) could lead to nearly as good route selection results, while measurement times are shorter.

9 Number of candidate routes

We now turn to the question of how many candidate routes a node should maintain in order to achieve the best possible PLE. As more candidate routes are added, especially routes with an individual PLE much worse than the PLE of the best candidate route, we can expect diminishing returns, or even a worsening of the PLE.

First, we run a one-week test comparing the performance of having *c* candidate routes in a node, with *c* in the range 1-4. The *c* candidate routes used by a node are always the *c* best (lowest PLE) routes identified in the test of section 7. A node first tries the best candidate route twice, and then tries the other candidate routes in from best-to-worst order. If the message is still not delivered, it tries the best route twice again, etc. The result of this test is that having multiple candidate routes outperforms having only one candidate route. However, after sending 100.000 test messages for each *c* for each node, we find no statistically significant difference in the PLE(200 ms) for 2, 3, and 4 candidate routes. In practical terms, having 2 candidate routes is as good as having 4 in this test.

In a second one-week test, we studied the performance of multiple candidate routes if all candidate routes are 'long' 2-hop routes. We eliminated the direct route to node 0, and the route via node 2 which has one very short hop, as candidates, and ran the test again with the remaining best routes. The results are therefore somewhat indicative of the PLE that can be expected in a larger test network, for nodes that are too far away from node 0 to reach it with a single hop. Figure 9 shows the test results. For node 5, we see a clear improvement in PLE(200 ms) when more candidate routes are added. For all other nodes, these is an improvement when going from 1 candidate route to multiple routes, but again no statistically significant differences for 2, 3, and 4 candidate routes. Figure 10 shows averages for the test results in figure 9.

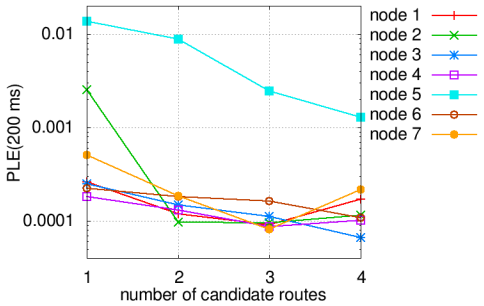

Figure 9 PLE(200 ms) for 'long' 2-hop routes only.

We conclude that in a dense network, for example the network of figure 1 but with node 5 excluded, keeping 2 candidate routes will be sufficient, and this can keep routing tables small. A more general networking solution should however have the ability to maintain more than 2 candidate routes, to optimize the PLE for relatively isolated nodes like node 5.

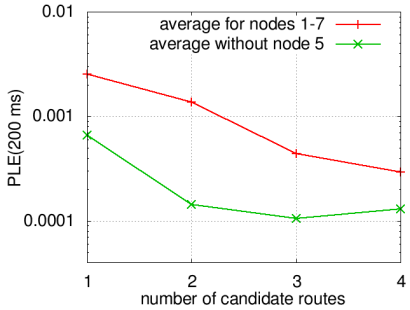

Figure 10. Average PLE(200 ms) for 'long' 2-hop routes.

For routing via long 2-hop nodes only, figure 9 shows a best-case PLE(200 ms) of about 0.0001, which is high compared to the PLE(200 ms) values found in the test of figure 3, where direct routing to node 0 is allowed. Apparently, another factor than multipath fading is dominant in determining the value of the best case PLE(200 ms). It might be possible to lower the influence of this factor by re-tuning the system, for example by changing WT, de-

creasing the message sending rate per node (which lowers system self-interference), or changing the MAC parameters. This is a topic for further study.

10 Conclusions

To make 802.15.4 control networks acceptable as a replacement for wired control, we must look into the way that end users experience the latency characteristics of the network. Based on this consideration, we have introduced a latency measure PLE, and optimized PLE(200 ms) based on measurements done during working hours in an office environment. Test runs lasting at least a week were done with most links in the clear region. The test results indicate that each node should maintain a list of multiple candidate routes that it can use to deliver a message. We have shown in [21] that candidate route information can be created and stored in advance. Only infrequent updates are necessary to adapt to changes that occur over timescales of weeks.

Compared to most WSN test networks in literature, our test network has a much higher node density, as we expect multiple wireless sensors and actuators per room. This leads to a system where, if the retry strategy in the protocol is designed well, low link quality is no longer a dominant cause of latency deadlines being exceeded. Instead, for PLE(200 ms), multi-path cancellation becomes a dominant cause [21], which can be eliminated by using multiple candidate routes. When this cause is eliminated, the presence or absence of a clear-region 1-hop link to the destination becomes a major determinant. We have some tentative evidence that system self-interference will become a significant determinant at some point above an average rate of 40 packets per second in the network, not counting MAC acknowledge packets. This high average packet rate is unrealistic in a small building control network, but might be approached in a large control network that needs to use multi-hop routes often to deliver messages. It is likely that the introduction of an exponential back-off in the invoking the MAC will improve worst-case latency under higher network loads.

Some interesting topics for future investigation are:

- Optimal WT values for multi-hop routes
- Quantification of an acceptable load
- Effects of changing the carrier sense and retry parameter settings at the MAC level

11 Literature

[1] J. Zhao, and R. Govindan, *Understanding Packet Delivery Performance in Dense Wireless Sensor Networks*, SenSys 2003.

[2] A. Woo, T Tong, D. Culler, *Taming the Underlying Challenges of Reliable Multihop Routing in Sensor Networks*, SenSys, 2003.

[3] IEEE Computer society, part 15.4, *Wireless medium Access Control (MAC) and Physical Layer (PHY) Specifications for Low Rate Wireless personal Area networks (LRWPAN),* Institute of Electrical and Electronics Engineers, Inc, 2003.

[4] J-S. Lee, *An Experiment on Performance Study of IEEE 802.15.4 Wireless Networks, ETFA 20*05.

[5] O. Hyncica, P. Kacz, P. Fiedler, Z. Bradac, P. Kucera, and R. Vrba, *The Zigbee Experience,* ISCCSP 2006.

[6] M. Petrova, J. Riihijarvi, P. Mahonen, and S. Labella, *Performance Study of IEEE 802.15.4 Using Measurements and Simulations,* WCNC 2006.

[7] M.M. Holland, R.G Aures, W.B. Heinzelman, *Experimental Investigation of Radio Performance in Wireless Sensor Networks,* 2nd IEEE workshop on wireless mesh networks, 2006.

[8] M. Zuniga, and B. KrishnamaChari, *Analyzing the Transitional Region in Low-Power Wireless Links*, SECON, 2004.

[9] D. Kotz, C. Newport, R. Gray, J. Liu, Y. Yuan. and C. Elliott, *Experimental evaluation of wireless simulation assumptions*, Dartmouth Computer Science Technical report, TR2004-507, June 2004.

[10] A. Cerpa, J.L. Wong, M. Potkonjak, D. Estrin, *Temporal Properties of Low Power Wireless Links: Modeling and Implications on Multi-Hop Routing*, MobiHoc, 2005.

[11] A. Meier, *Safety-Critical Wireless Sensor Networks*, PhD thesis 18451, ETHZ, 2009.

[12] D.S.J. de Couto, D. Aguayo, B.A. Chambers, R. Morris, *Performance of Multihop Wireless Networks: Shortest Path is Not Enough,* ACM SigComm communications review, Vol 33, No 1, 2003.

[13] K. Srinivasan, P. Dutta, A. Tavakoli, P. Levis, *Understanding the Causes of Packet Delivery Success and Failure in Dense Wireless Sensor Networks*, Technical Report SING-06-00, 2006.

[14] G. Zhou, T. He, S. Krishnamurthy, and J.A. Stankovic, *Impact of Radio Irregularity on Wireless Sensor Networks,* MobiSys '04, June 2004.

[15] Y. Wang, M.C. Vuran, S. Goddard, *Cross-layer analysis of the End-to-end Delay Distribution in Wireless Sensor Networks*, 30th IEEE RTSS, 2009.

[16] T. He, J.A. Stankovic, C. Lu, T. Abdelzaher, *"SPEED: a stateless protocol for real-time communication in sensor networks,* ICDCS-23, 2003.

[17] M. Soyturk, D.T. Altilar, *Reliable Real-Time Data Acquisition for Rapidly Deployable Mission-Critical Wireless Sensor Networks*, IEEE INFOCOM, 2008

[18] R. S. Oliver, G Fohler, *Probabilistic Routing for Wireless Sensor Networks*, 29th IEEE Real-RTSS WiP 2008.

[19] K. Holtman. *Long-duration Reliability Tests of Low Power Wireless Sensing and Control Links in an Office Environment*. In: ARCS 2010 Workshop Proceedings of the 23th Int. Conf. on Architecture of Computing Systems 2010, pp 259-258.

[20] http://www.jennic.com/

[21] K. Holtman; P. van der Stok. *Routing recommendations for low-latency 802.15.4 control networks.* In: ARCS 2011 Workshop of the 24th Int. Conf. on Architecture of Computing Systems 2011, pp 285-290.

Quantifying the Channel Quality for Interference-Aware Wireless Sensor Networks

Claro Noda, Shashi Prabh, and Mário Alves
CISTER Research Unit, ISEP
Instituto Politécnico do Porto
Porto, Portugal
{cand, ksp, mjf}@isep.ipp.pt

Carlo Alberto Boano
Universität zu Lübeck
Lübeck, Germany
cboano@iti.uni-luebeck.de

Thiemo Voigt
Swedish Institute of Computer Science
Kista, Sweden
thiemo@sics.se

***Abstract*—Reliability of communications is key to expand application domains for sensor networks. Since Wireless Sensor Networks (WSN) operate in the license-free Industrial Scientific and Medical (ISM) bands and hence share the spectrum with other wireless technologies, addressing interference is an important challenge. In order to minimize its effect, nodes can dynamically adapt radio resources provided information about current spectrum usage is available.**

We present a new channel quality metric, based on availability of the channel over time, which meaningfully quantifies spectrum usage. We discuss the optimum scanning time for capturing the channel condition while maintaining energy-efficiency. Using data collected from a number of Wi-Fi networks operating in a library building, we show that our metric has strong correlation with the Packet Reception Rate (PRR). This suggests that quantifying interference in the channel can help in adapting resources for better reliability. We present a discussion of the usage of our metric for various resource allocation and adaptation strategies.

***Index Terms*—ISM Bands, Interference, Dynamic Resource Adaptation, Forward Error Correction, Cross-Layer Optimizations, Wireless Sensor Networks**

I. Introduction

Wireless technologies have grown exponentially during the last decade and are progressively cast around for more applications. Many standardized technologies operate in crowded license-free Industrial Scientific and Medical (ISM) frequency bands. Wireless networks in these bands are now ubiquitous in residential and office buildings as they offer great flexibility and cost benefits. However, despite the extensive research, the issue of reliability of wireless networks remains a challenge. Medium access techniques such as TDMA and FDMA cannot be readily applied in the context of ISM bands [1], as they are not designed to tolerate inter-network interference. Instead, distributed multiple access schemes based on *carrier sense*, such as CSMA, are widely employed along with Spread Spectrum modulation techniques which provide some robustness as well as generate lower levels of interference. Although this bottom-up approach to unlicensed spectrum usage exacerbates the challenges to achieve reliability and predictability in low-cost wireless solutions, there are many gains for end users [2] and extensive opportunities for innovation [3]. It has also incubated new research directions, such as dynamic spectrum allocation for future wireless systems [4]. Inspired by this paradigm, we investigate mechanisms for interference avoidance within ISM bands for low-power radios.

Wireless Sensor Networks (WSN) are seen as a viable alternative for monitoring, control and automation applications, provided they are made appropriately reliable and delays are bounded. To this end, interference and coexistence pose a major challenge. In this paper, we present the *Channel Quality* (CQ) metric that provides a quick and accurate estimate of interference by capturing a channel's availability over time at a very high resolution. This metric is useful towards achieving better reliability and lower latency through dynamic radio resources allocation.

Interference from coexisting networks in ISM Bands is typically referred as Cross Technology Interference (CTI). Even though CTI represents a well known problem [5–8] it has not been adequately addressed in WSN. This problem is hard to resolve for two reasons: a) efficient cooperative schemes for spectrum access are not possible with currently deployed technologies and b) there are large RF power and spectrum footprint asymmetries. CTI could be avoided by sophisticated communication protocols that are sensitive to instantaneous spectrum occupation. However, low-cost hardware and limited energy-budget of the nodes make the typical spectrum sensing techniques as proposed for non resource constrained systems [9] unsuitable for WSN.

This paper has the following contributions:

- A novel channel quality metric that is based on channel availability and is agnostic to the interference source.
- An analysis of the parameter space and validation of the metric's performance with real-world interference traces.

The rest of this paper is organized as follows. Section II provides further motivation for this work and in Section III we derive the expression for our CQ metric. Section IV describes how we use the energy detection (ED) feature in IEEE-802.15.4 compliant radios to measure evolution of signal (interference) strength in 802.15.4 channels, our experimental setup and our data collection experiments. We then discuss results of our evaluations and conclude the paper in Section V.

II. Motivation

Any given network configuration at deployment phase, like channel selection, is typically not enough as the network

may experience communication interruptions or simply fails at some point. We need WSN that seamlessly adapt resources and self-organize to maintain their integrity in a changing environment. Several recent studies have addressed burstiness and interference in wireless links. Srinivasan et al. proposed a metric to quantify link burstiness and show impact on protocol performance and achievable improvements in transmission cost [10]. Also, Munir et al. investigated scheduling algorithms to improve reliability and provide latency bounds [11]. However, these solutions can not react to instantaneous changes in the channel condition. They rather select routes and channels using long-term observations.

There are aggressive techniques to deal with interference in wireless systems. Successive Interference Cancellation (SIC) has been partially demonstrated for 802.15.4 in Software Defined Radios [12]. Nevertheless, there are practical limitations to advance with it. For example, it is known that SIC requires highly linear amplifiers in the receiver (large dynamic range) and also excellent adjacent channel suppression, because residual energy put in the front-end causes it to underperform and desensitizes the radio. Both of these requirements lead to expensive solutions. Furthermore, it is questionable whether SIC's demand for signal processing could outweigh its benefits compared to other approaches, in view of available technology, inexpensive hardware and energy budget constrains. Finally, these ideas are not trivially applied to CTI because a large heterogeneous set of possible signals to disentangle further complicate SIC-based solutions.

Alternatively, we advocate modest improvements in low-power receiver architecture can enable energy efficient spectrum sensing, which is necessary for nodes to form smart reactive networks that eliminate the need for highly complex radios. Spectrum occupation can change rapidly in time and space, yet under unfavourable channel conditions nodes adapt resources or find better channels to maintain communications. Dynamic resource adaptation can lower latency bounds and boost reliability but in order to encompass this information into protocols one needs accurate spectrum sensing. In this paper we show that sufficiently accurate spectrum sensing is feasible with sensor nodes.

Currently, the radio transceivers in WSN nodes are mostly based on the IEEE-802.15.4 standard that is intended for low-power operation. On reception, off-the-shelf radios require around 50 mW and consume 200 – 2000 μJ per packet received. This power is drawn by the PLL synthesizer, digital demodulator, symbol decoder and RF analog blocks for signal filtering, amplification and down-conversion among other functions, typically in this order. Recent incursions in 0.18 μm CMOS process of PLL realizations [13–16], targeted for these systems, report fairly appealing figures: power consumptions below 3 mW and lock-in times less than 30 μs. Since the PLL synthesizer is known to be by far the most power-hungry block in the receiver, these results suggest that the next generations of WSN radios would require, at least, one order of magnitude less chip energy per bit received.

Now, in order to support ED spectrum sensing only the PLL synthesizer, analog RF blocks plus AGC are necessary, while the demodulator can be turned off. Interestingly, among other optimizations, this further reduces energy consumption while the receiver is used exclusively to detect the RF energy in the channel, but we have not yet found any 802.15.4 radio chip providing this flexibility.

III. Channel Quality Metric

The source of interference in wireless networks are typically very diverse. Interference causes a decrease in the Signal-to-Noise plus Interference Ratio (SNIR) which can result in packet losses. Any device that produces RF signals with spectral components within or near the receiver passband is a potential interferer. Average energy in a channel has been used as an indicator of channel usage in the previous literature [17, 18]. Unfortunately, this metric is unable to distinguish between a channel where the traffic is bursty with large inactive periods and a channel that has very high frequency periodic traffic with the same energy profile. Clearly, the first scenario is preferable. It may well be the case that the traffic in the second case consists entirely of short-duration peaks resulting in much lower average energy but unusable channel. Motivated by this observation, we propose a metric that is based on the fine-grained availability of the channel over time and ranks channels with larger inactive periods, or vacancies, more favourably.

Consider the energy levels (or RSSI) in some channel are measured periodically with period P. Suppose, the acceptable noise level and interference threshold is R_{THR}. Therefore, the channel can be considered idle when $RSSI < R_{THR}$. For example, Figure 1 shows RSSI samples over time along with idle intervals, which we refer as *channel vacancies* (CV). Let m_j denote the number of CV made of consecutive j idle samples and n the total number of samples. Then $m_1 + m_2 + \ldots + m_n = m$ is the total number of observed CV. Notice that j consecutive clear channel samples imply that the channel was idle for at least $(j-1)P$ time units. We define the average *channel availability* (CA) as:

$$CA(\tau) = \frac{1}{n-1} \sum_{j|(j-1)P>\tau} j m_j \qquad (1)$$

where $\tau > 2P$ is the time window of interest, which could be the duration of transmission of packets. As we argued earlier, a channel where $m_{2j} = k$ is more desirable than a channel where $m_j = 2k$, although jm_j is the same for both cases. In other works, we want to rank a channel with larger vacancies higher even though the sum of the idle durations might be the same. Hence, we define the *Channel Quality* metric as:

$$CQ(\tau) = \frac{1}{(n-1)} \sum_{j|(j-1)P>\tau} j^{(1+\beta)} m_j, \qquad (2)$$

where $\beta > 0$ is the bias. CQ in equation (2) take values between 0 and n^β, where the larger values indicate better channels. Observe that this expression is agnostic to the interference source. For example, Figures 1(a)-(b) show channel

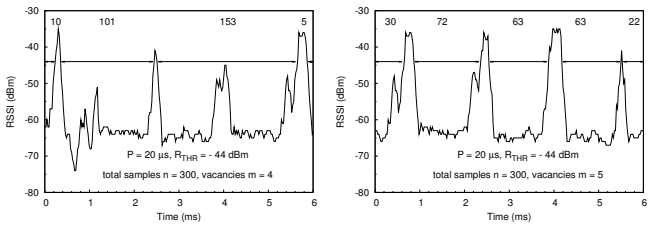

(a) (b)

Fig. 1. Channel vacancies: two scenarios with the same CA

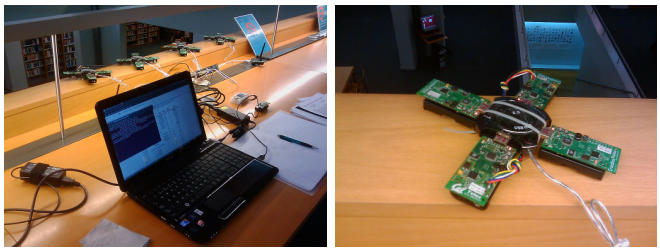

(a) (b)

Fig. 2. The experimental setup used to collect energy level traces on IEEE-802.15.4 channels deployed at the Library of the Faculty of Engineering at the University of Porto (a) and detail of TelosB motes arranged in a USB hub (b).

vacancies with $R_{THR} = -44$ dBm. The channel availability is similar in both cases ($CA_a = 0.88$ in Figure 1(a) and $CA_b = 0.83$ in Figure 1(b)), but due to less collisions the probability of correct reception is higher in the case of scenario in Figure (a) than that in Figure (b).

IV. Evaluation

In this section, we first describe our experimental set-up used for data collection followed by an analysis of our metric when applied to the data. We devise off-line experiments and implement them in Python [19] scripts to be run over the traces. This has the advantage of producing a naturally controlled environment, e.g. isolating channel effects that are present in an online experiment. We show that our metric is highly correlated with PRR.

A. Experimental Setup

In order to experimentally investigate our proposal we need traces of interference signals that help understand channel degradation in real-world settings. More specifically, we want to find out how our metric can help identifying a usable channel and eventually establish which alternative techniques can be applied to employ it effectively. Therefore, we have designed an experimental setup to study interference in the 2.4 GHz ISM band. This band is available globally; there are thousands of certified devices on the market that operate in it and coexistence problems are well known [5, 6], which ultimately facilitates the task of collecting interference traces. Our setup has no limitations to study any kind of interference, but given that Wi-Fi has been identified as the most critical interference source to affect WSN [6] and it is also widely available, in this paper we report experiments with traces where interference stems solely from Wi-Fi networks.

In our setup we scan all 16 802.15.4 channels simultaneously. We employ a set of 17 TelosB sensor nodes. In order to do multiple channel readings simultaneously we use one of the motes to transmit a scanning beacon on channel 26, which instructs all other nodes to switch to their respectively assigned channels and begin scanning. The motes are connected via USB hubs to a laptop as shown in Figure 2. We sample RSSI values at 40 kS/s on the CC2420 transceiver and store them in a memory buffer up to the largest possible number of samples. After completing 5600 samples, in approximately 130 ms, all nodes return to listen on channel 26 and wait for the next scanning beacon, in 8 seconds, while all RSSI readings we kept in the memory buffer are dumped to a file. Having one node per channel enables us to increase the pace at which data is collected and makes it easy to organize the log files.

A large density of Access Points capable of producing notorious spectrum occupation is mainstream in many metropolitan areas today and particularly in university campus. However, it is the density of users and the overall volume of data been transferred that actually produces congestion. Thus, we used our ensemble to collect measurements in our laboratory, which has moderate traffic on a few 802.15.4 channels. Then we conducted a measurement campaign at the Library of the Faculty of Engineering of the University of Porto, where we found very heavy traffic from 802.11 Wi-Fi networks. In our experiments, signals are well above the noise floor (10 - 70 dB), but more relevant is the time distribution of burst patterns that varies from a few microseconds to tens of milliseconds. To examine our metric proposal we then perform off-line experiments, upon a set of traces from a four hour capture.

B. Sampling Time

One of the questions we seek to answer is *how long* should we sample a channel in order to have a meaningful CQ value. Sampling too shortly leads to uncertainty about the near future state of the channel. Notice that the *clear channel assessment* (CCA) used in Carrier Sense Multiple Access with Collision Avoidance (CSMA/CA) mechanism would not help here given the asymmetric scenario in transmission power and spectral footprint [see 8]. Basically, such asymmetries in the PHY layer among different radios, make the distributed coordination approach fail. WSN nodes employ orders of magnitude less RF power than other channel contenders, which makes them more vulnerable to packet corruption since it is improbable that other nodes would detect an ongoing transmission and thus defer theirs. For this reason, it is necessary to sample for longer time, definitely larger than a CCA accounting for 8 symbol periods or 128 μS, in order to capture a sequence of events large enough to estimate the probability of successful packet reception.

On the other extreme, sampling too long introduces a cumulative effect that misses the dynamics of the channel availability and leads to poor prediction of the next state of the channel. The more distant in time the events are the

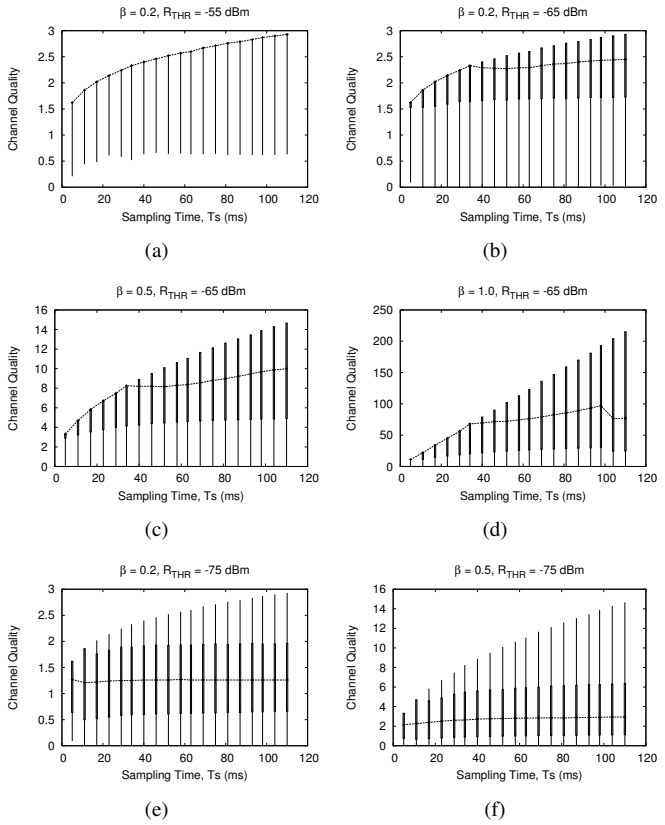

Fig. 3. CQ computed over all traces for different sampling times. The curves represent the median, boxes represent the interquartile range and bars stand for the rest of the values

more likely is that their probabilities are independent and therefore does not help to estimate the channel condition either. Furthermore, during the sampling period the radio is turned on which consumes energy.

In praxis this means that we need to find a compromise for the sampling time that is intrinsically dependent on the system observed.

In order to understand this compromise we progressively compute CQ, up to 120 ms, over all traces. Figure 3 illustrates the results which depend, primarily, on the threshold R_{THR}. Since we are not interest here in any specific packet duration, we chose $\tau = 0.2$ ms, small enough so that most CV contributions count in Equation 2. One common trend in all graphs is that CQ stabilizes after some time, provided there is sufficient interference. This indicates that Equation 2 converges toward a value that is proportional to an average number of vacancies during the sampling period and, clearly, also depends on β and the values of j.

As can be seen in Figure 3, the heavier the interference the faster CQ stabilizes. On the contrary, if the channel is mostly idle (e.g. $R_{THR} = -55$ dBm as in 3(a)), CQ grows – up to n^{β}– with very high probability. An intermediate case, as when CQ is computed for -65 dBm, see 3(b)-3(d), demonstrates that the metric typically grows to a certain value until it finally stabilizes. Hence, these sampling times are much smaller that

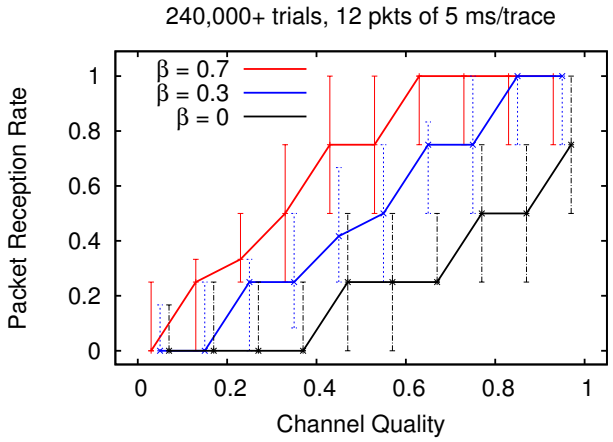

Fig. 4. PRR and CQ computed according to Equation 3

the time scale of the interference pattern present in the channel. Based on this behaviour, an optimum sampling time would be as long as it is necessary to have the median of CQ stabilized.

In a system where this metric is computed online the sampling time, represented by n in Equation 2, could be dynamically maintained at this turning point where the median of CQ stabilizes, or below a certain maximum value. We defer the development of a control algorithm for this purpose to future work. For the rest of experiments we use hand-picked scanning times, smaller than 40 ms, based on our exploration of these traces.

C. Correlation with PRR

We now investigate how the channel availability as described by our CQ metric is related to the probability of successful packet receptions. For this experiment we use a third of each RSSI trace, lasting 130 ms, to compute the metric and the remaining to check for the presence of interference that may lead to packet corruption. If the RSSI readings remain under a predetermined value R_{THR} during the duration of each packet, then the packet is considered successfully received. Actually for correct reception a signal to interference margin is required. This is known as the Co-channel Rejection Ratio and is defined for each radio. Multiple packets are transmitted over each trace and the average is computed for PRR. Packets are transmitted periodically and transmissions are separated by an inter-packet interval $IPI = 1$ ms. In this way, we conduct an experiment with 240,000+ off-line packet verifications on traces obtained from the library with Wi-Fi interference and using an RSSI threshold of -65 dBm.

As shown in the previous section, Equation 2 provides a range for CQ values that depends on n and β. However, in order to compare among CQ values computed with different parameter values we rewrite CQ as:

$$CQ(\tau) = \frac{1}{(n-1)^{(1+\beta)}} \sum_{j|(j-1)P>\tau} j^{(1+\beta)} m_j, \qquad (3)$$

CQ in Equation (3) now take values between 0 and 1, regardless of n and β values. For example, if we compute

Equation 3 with $\beta = 0.3$ for an 802.15.4 ACK frame lasting 352 μs, in the scenario in Figure 1(a) and (b) we obtain $CQ_a = 0.65$ and $CQ_b = 0.50$, which are more accurately reflect the difference among the two channels than previous values from Equation 1.

Figure 4 shows the results where we find a strong correlation with PRR. The curves correspond to the median and the error bars represent the interquartile range computed over the entire set of traces. We compute CQ for bias (β) values 0, 0.3 and 0.7 to highlight that $\beta = 0.3$ linearises the curves. Notice, $\beta = 0$ is equivalent to average *channel availability* as described by Equation 1. In this case CQ values grow faster than PRR which indicates that despite channel been less occupied there are still many collisions that hinder PRR values. As we increase β, this selectively raises CQ favouring larger CV to have more weight in the sum.

This is an interesting result, as been able to tune β and maximize the correlation among PRR and CQ makes this metric an accurate indicator of the channel condition. Similar to the scanning time, an algorithm to find a value for β that is optimum is left out of this paper.

D. Discussion

In this section we revisit some resource adaptation techniques and discuss how they could be dynamically applied to leverage our CQ metric for interference-aware communication protocols.

Lin et al. demonstrated a novel pairwise transmission power control for WSN that performs significantly better than node-level or network-level power control methods [20]. They improve PRR and energy consumption by dynamically adapting the RF transmission power to maintain the minimum level required to guarantee a good link. This is a clever approach to compensate for the non-linear pathloss. However, it does not account for two important aspects: a) the irreducible error floor [21, Ch. 6] produced by fading can not be removed by increasing transmission power and b) it does not address external interference. A solution to both these problems is dynamic frequency and power adaptation, simultaneously.

In this regard, one can augment such pairwise power control mechanism with CQ, directly establishing a dynamic lower bound for the RF power to use in the transmitter, previous to actual transmissions. Besides, since maximum transmission power can not be exceeded, an alternative such as a moving to a different channel may be inferred immediately. Starting from the RSSI samples in memory, we could ask the question: which signal level would result in a CQ value that satisfies a given requirement for channel usage under the current interference level?

In general, protocols designed for multichannel operation can maintain good links using a channel ranking with distributed CQ computations, among neighbour nodes, provided a control channel among them is stable. Additionally, this could aid topology changes when interferers spectral footprint is very large, as in 802.11n, to take advantage of the irregular coverage, common in some indoor environments.

Successful transmissions in the scenarios in Figure 1 also depend on the packet size. Certain packet size would maximize throughput or minimize the time to deliver a data object over the channel, for a given interference level. Observe that shorter packets have better chances of avoiding collisions (and hence retransmissions) but also result in higher overhead due to fixed packet headers and acknowledgement delays. One could look into the relationship between these optimum packet sizes and the CQ values computed on the channel. Similar to the PRR correlation in Figure 4, there would be a value of β that linearises such dependency. Based on observed CQ values protocols can then tune packet size to transfer data in a minimum time.

FEC techniques pose a trade-off between data recovery capacity and its inherent payload and computation overhead. Recently, Liang et al. demonstrated the Reed-Solomon (RS) correcting codes performs well while recovering packets affected by 802.11 interfering signals [8]. Since interference levels may vary extensively it is interesting to see if this solution can benefit from simple CQ based optimizations.

On the other hand, energy cost to compute the CQ metric must be further explored in view of overall energy balance in dynamic resource adaptation. In future work we plan to extend our experiments and later implement the metric on WSN hardware.

V. Conclusions

We introduced a new channel quality metric that is based on the availability of the channel over time. The metric is useful for interference aware protocols in WSN. We described our experimental setup for collecting real-world interference traces in the 2.4 GHz ISM band. Using this data, we showed that our metric has strong correlation with PRR. Thus, our metric's characterization of a channel is reliable and applicable in practice. We also discussed dynamic resource allocation techniques for interference-aware protocols in WSN for which our metric can prove to be useful. We are currently working on a software implementation of CQ for WSN hardware to further validate its performance in online experiments.

References

[1] Kenneth R. Carter. Unlicensed to kill: a brief history of the Part 15 rules. *Info*, 11(5):8–18, 2009. ISSN 1463-6697.

[2] Henry Goldberg. Grazing on the commons: the emergence of Part 15. *Info - The journal of policy, regulation and strategy for telecommunications*, 11(5):72–75, 2009. ISSN 1463-6697.

[3] Vic Hayes and Wolter Lemstra. Licence-exempt: the emergence of Wi-Fi. *Info - The journal of policy, regulation and strategy for telecommunications*, 11(5): 57–71, 2009. ISSN 1463-6697.

[4] Ian F. Akyildiz, Won-Yeol Lee, Mehmet C. Vuran, and Shantidev Mohanty. Next generation/dynamic spectrum

access/cognitive radio wireless networks: A survey. *Computer Networks*, 50(13):2127 – 2159, 2006. ISSN 1389-1286.

[5] A. Sikora and V. Groza. Coexistence of IEEE 802.15.4 with other systems in the 2.4 GHz-ISM-Band. In *IEEE Instrumentation and Measurement Technology*, pages 1786–1791, Ottawa, Canada, May 2005.

[6] M. Petrova, L. Wu, P. Mahonen, and J. Riihijarvi. Interference Measurements on Performance Degradation between Colocated IEEE 802.11g/n and IEEE 802.15.4 Networks. In *International Conference on Networking (ICN)*, Sainte-Luce, Martinique, April 2007. ISBN 0-7695-2805-8.

[7] Jan-Hinrich Hauer, Andreas Willig, and Adam Wolisz. Mitigating the Effects of RF Interference through RSSI-Based Error Recovery. In Jorge Silva, Bhaskar Krishnamachari, and Fernando Boavida, editors, *Wireless Sensor Networks*, volume 5970 of *Lecture Notes in Computer Science*, chapter 15, pages 224–239. Springer Berlin / Heidelberg, Berlin, Heidelberg, 2010. ISBN 978-3-642-11916-3.

[8] Chieh-Jan Mike Liang, Bodhi Priyantha, Jie Liu, and Andreas Terzis. Surviving Wi-Fi Interference in low-power ZigBee Networks. In *Proceedings of the 8th ACM Conference on Embedded Networked Sensor Systems (SenSys'10)*, pages 309–322, Zurich, Switzerland, November 2010.

[9] T. Yucek and H. Arslan. A Survey of Spectrum Sensing Algorithms for Cognitive Radio Applications. *IEEE Communications Surveys Tutorials*, 11(1), 2009.

[10] Kannan Srinivasan, Maria A. Kazandjieva, Saatvik Agarwal, and Philip Levis. The beta-factor: measuring wireless link burstiness. In *SenSys*, pages 29–42, 2008.

[11] Sirajum Munir, Shan Lin, Enamul Hoque, S. M. Shahriar Nirjon, John A. Stankovic, and Kamin Whitehouse. Addressing Burstiness for Reliable Communication and Latency Bound Generation in Wireless Sensor Networks. In *ACM/IEEE IPSN*, pages 303–314, Stockholm, Sweden, April 2010.

[12] Daniel Halperin, Thomas Anderson, and David Wetherall. Taking the sting out of carrier sense: interference cancellation for wireless LANs. In *Proceedings of the 14th ACM international conference on Mobile computing and networking*, MobiCom '08, pages 339–350, New York, NY, USA, 2008. ACM. ISBN 978-1-60558-096-8.

[13] M. Vamshi Krishna, J. Xie, W.M. Lim, M.A. Do, K.S. Yeo, and C.C. Boon. A low power fully programmable 1MHz resolution 2.4GHz CMOS PLL frequency synthesizer. In *Biomedical Circuits and Systems Conference, 2007. BIOCAS 2007. IEEE*, pages 187 –190, 2007.

[14] Louis-François Tanguay and Mohamad Sawan. An ultra-low power ISM-band integer-n frequency synthesizer dedicated to implantable medical microsystems. *Analog Integr. Circuits Signal Process.*, 58:205–214, March 2009. ISSN 0925-1030.

[15] Wu Xiushan, Wang Zhigong, Li Zhiqun, Xia Jun, and Li Qing. Design and realization of an ultra-low-power low-phase-noise CMOS LC-VCO. *Journal of Semiconductors*, 31(8):085007, 2010.

[16] Geng Zhiqing, Yan Xiaozhou, Lou Wenfeng, Feng Peng, and Wu Nanjian. A low power fast-settling frequency-presetting PLL frequency synthesizer. *Journal of Semiconductors*, 31(8):085002, 2010.

[17] Federico Penna, Claudio Pastrone, Maurizio A. Spirito, and Roberto Garello. Measurement-Based Analysis of Spectrum Sensing in Adaptive WSNs under Wi-Fi and Bluetooth Interference. In *VTC Spring*. IEEE, 2009.

[18] Luca Stabellini and Jens Zander. Energy-efficient Detection of Intermittent Interference in Wireless Sensor Networks. *Int. J. Sen. Netw.*, 8:27–40, July 2010. ISSN 1748-1279.

[19] Guido Van Rossum. Python for Unix/C Programmers. In *Proc. of the NLUUG najaarsconferentie. Dutch UNIX users group*, 1993.

[20] Shan Lin, Jingbin Zhang, Gang Zhou, Lin Gu, John A. Stankovic, and Tian He. ATPC: adaptive transmission power control for wireless sensor networks. In Andrew T. Campbell, Philippe Bonnet, and John S. Heidemann, editors, *SenSys*, pages 223–236. ACM, 2006. ISBN 1-59593-343-3.

[21] Andrea Goldsmith. *Wireless Communications*. Cambridge University Press, New York, NY, USA, 2005. ISBN 0521837162.

Existing offset assignments are near optimal for an industrial AFDX network

Xiaoting Li, Jean-Luc Scharbarg, Christian Fraboul
INP-ENSEEIHT IRIT, Université de Toulouse
Toulouse, France
{*Xiaoting.Li, Jean-Luc.Scharbarg, Christian.Fraboul*}*@enseeiht.fr*

Frédéric Ridouard
LISI-ENSMA, University of Poitiers
Poitiers, France
frederic.ridouard@ensma.fr

***Abstract*—Avionics Full DupleX Switched Ethernet (AFDX) has been developed for modern aircraft such as Airbus 380. Due to the non-determinism of switching mechanism, a worst-case delay analysis of the flows entering the network is a key issue for certification reasons. Up to now most existing approaches (such as Network Calculus) consider that all the flows are asynchronous and they do not take into account the scheduling of flows generated by the same end system. It is then pessimistic to take into account such a synchronous scenario. Each end system can be considered as an offset free system, thus the main objective of this paper is to evaluate existing offset assignments in the context of an industrial AFDX network. Existing offset assignments are adapted to take into account specific characteristics of an AFDX network. Worst-case delay results are obtained according to these offset heuristics. It is shown that some existing heuristics are not efficient while some are near optimal for the studied industrial AFDX network.**

***Keywords*-AFDX network, offset assignment, worst-case delay**

I. Introduction

Avionic Full DupleX Switched Ethernet (AFDX [1]) has been proposed in order to satisfy the growing requirements of avionics application. Such a network is defined based on static network configuration and routing. The demonstration of a determined upper bound for end-to-end (ETE) communication delays on such a real-time network plays a key role. Different methods [2]–[5] have been presented for the worst-case delay analysis on the AFDX network. Among them, the Network Calculus [6] has been used for the certification of Airbus 380.

Since each end system of the AFDX network schedules its flows according to a local clock, it is pessimistic to consider that all frames arrive simultaneously (synchronous scenario) on this network. This issue has been addressed in [7], in which a computation method integrating the offsets of flows based on the Network Calculus approach has been developed. However, only one offset assignment originally designed for the CAN network in [8] was applied to an industrial AFDX network. It is interesting to consider other existing offset assignments [9], [10] in order to find the best algorithm for an industrial AFDX network. Moreover, the existing algorithms can be adapted in order to take into account specific characteristics of an AFDX network.

The objective of this paper is to evaluate and compute offset assignment algorithms for an industrial AFDX network. The goal of the evaluation is to measure the gap between offset assignment based on heuristics and the optimal assignment, which is intractable on an industrial AFDX network. An upper bound on this gap is computed, based on an optimal scenario.

This paper is organized as follows. Section II shortly introduces the context of the studied industrial AFDX network and existing offset assignments. Section III derives an ideal offset assignment which gives an optimal scenario for the scheduled flows. In Section IV, new heuristics integrating the AFDX characteristics are proposed. The existing and proposed offset assignments are applied to the industrial AFDX network, and their results are compared and analyzed in Section V. Section VI concludes and indicates directions for future research.

II. Context

A. Introduction of the industrial AFDX network

An AFDX network [1] is composed of end systems and switches. The inputs and outputs of the AFDX network, called $end\ systems\ (ES)$, are connected by several interconnected AFDX switches. Each end system can be connected to only one port of an AFDX switch and each port of an AFDX switch can be connected at most to one end system. Links between switches work in full-duplex mode.

A $Virtual\ Link\ (VL)$ standardized by ARINC-664 is a concept of virtual communication channel, which statically defines the flows. A connection defined by a Virtual Link is unidirectional, including one source end system and one or more paths leading to different destination end systems (multicast nature). A VL is characterized by:

- $Bandwidth\ Allocation\ Gap\ (BAG)$, the minimum delay between two consecutive frames of corresponding VL ranging in powers of 2 from 1 ms to 128 ms, and
- S_{min} and S_{max}, the minimum and maximum frame length which respect the standard Ethernet frame.

An AFDX network architecture is illustrated by Figure 1. According to this architecture, there are five end systems and two AFDX switches. On the example, v_1 has a unique path $\{e_1 - S_1 - S_2 - e_4\}$ and v_5 has multi-paths $\{e_3 - S_2 - e_4\}$ and $\{e_3 - S_2 - e_5\}$.

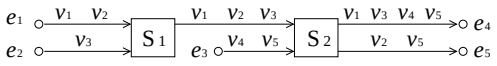

Figure 1. Example of an AFDX configuration

The industrial AFDX network interconnects aircraft functions in the avionics domain. It is composed of two redundant networks. Each network includes 123 end systems, 8 switches, 984 Virtual Links and 6412 VL paths (due to VL multicast characteristics). The left part in Table I gives the dispatching of VLs among BAGs. The right part in

BAG (ms)	Number of VL
2	20
4	40
8	78
16	142
32	229
64	220
128	255

Frame length (bytes)	Number of VL
0-150	561
151-300	202
301-600	114
601-900	57
901-1200	12
1201-1500	35
> 1500	3

Table I
BAGS AND FRAME LENGTHS

Table I gives the dispatching of VLs among frame lengths, considering the maximum length S_{max}. The majority of VLs considers short frames. Table II shows the number of VL paths per length (i.e. the number of crossed switches).

Nb of crossed switches	Number of paths
1	1797
2	2787
3	1537
4	291

Table II
VL PATHS LENGTHS

This industrial AFDX network works at 100 Mb/s and the technological latency of an AFDX switch is 16 μs. The overall workload (utilization) of the industrial network is about 10%. Actually, the industrial AFDX network is lightly loaded in order to guarantee that buffers will never overflow. Both sporadic VLs and periodic VLs exist on the AFDX network, and offsets can be assigned to periodic VLs. There is no global clock in an AFDX network. Consequently, frame releases of different end systems are independent. However, each end system schedules its flows. This scheduling can be integrated in the worst-case delay analysis thanks to offsets. The next paragraph gives an overview of existing offset assignments.

B. Existing offset assignments

The offset assignment has been studied in [9] in the context of periodic task sets executed in a uniprocessor. Each task τ_i is characterized by a period T_i, a hard deadline D_i, a processing time C_i and an offset O_i. In the context of uniprocessor, the systems can be classified into three classes in terms of offset:

- Synchronous system: all the tasks have the same fixed offsets, i.e., at time 0, all the tasks generate one request;
- Asynchronous system: an offset is allocated to each task due to application constraints;
- Offset free system: any offset can be allocated to each task in order to improve the system schedulability.

For the third class, a key point is the choice of an offset assignment. The number of possible offset assignments is exponential.

In [9], an *optimal offset assignment* is proposed to exhaust all possible non-equivalent offset assignments. Although this method reduces significantly the number of combinations, the number remains exponential. *Dissimilar offset assignment*, denoted GCD, is then defined in order to reduce computational complexity in the comparison with the *optimal offset assignment* by providing a single offset assignment for a task set. This method tries to move from the synchronous case as much as possible. It considers a minimal distance $\lfloor \frac{gcd(T_i,T_j)}{2} \rfloor$ between two requests of τ_i and τ_j, where $gcd(T_i, T_j)$ is the greatest common divisor of T_i and T_j. This method treats task pairs (τ_i, τ_j) by decreasing value of $gcd(T_i, T_j)$.

Near-optimal offset assignment heuristics are derived in [10] based on the study of GCD. This assignment considers four alternative offset allocations when GCD fails to generate a schedulable asynchronous situation. Since both these two approaches assign offsets to VLs pair by pair, they are called *PairAssign* in this paper. Besides the decreasing value of $gcd(T_i, T_j)$, other heuristics are proposed considering criteria like utilization rate, i.e., $\frac{C_i}{T_i}$, and the value of $-gcd(T_i, T_j)$ to decide the order of flow pairs. These four heuristics are denoted and defined as follows:

- $RateAdd$: $\frac{C_i}{T_i} + \frac{C_j}{T_j}$,
- $RAGCD$: $(\frac{C_i}{T_i} + \frac{C_j}{T_j}) \times gcd(T_i, T_j)$,
- $RMGCD$: $max(\frac{C_i}{T_i}, \frac{C_j}{T_j}) \times gcd(T_i, T_j)$;
- $GCDMinus$: $-gcd(T_i, T_j)$;

In [8], the authors addressed that the offset assignments mentioned above are not efficient when applied to the scheduling of automotive message, and an offset assignment algorithm is tailored for automotive CAN network. This algorithm, called *SingleAssign* in this paper, aims at choosing offsets to maximize the distance between frames. For n flows emitted by one source node, sort them by increasing value of their periods and calculate $T_{max} = \max_{i \in [1,n]}\{T_i\}$. The assignments start with the flow having smallest period and process one flow after another. For a flow τ_k ($k \in [1, n]$), its offset O_k is decided as follows:

- first search for the least loaded interval in $[0, T_k)$;
- then set O_k in the middle of this interval;
- finally record all the frames of τ_k released in $[0, T_{max})$.

III. Optimal scenario of scheduled flows over the AFDX network

Considering an industrial AFDX configuration with about 1000 flows, the *optimal offset assignment* proposed in [9] is intractable. Thus approaches based on heuristics have to be used. Then, the evaluation of the gap between the *optimal offset assignment* and the assignment generated by each heuristics is an important issue. For a given flow, this gap can be defined as the difference between the worst-case ETE delays obtained by, on the one hand considering the *optimal offset assignment*, on the other hand considering the offset assignment based on a heuristic. On a whole configuration, the gap is the average of the gaps obtained for the flows. Obviously, it is not possible to compute the gap for the *optimal offset assignment* on an industrial AFDX configuration, since the *optimal offset assignment* is intractable. Then, a first idea is to compute an upper bound on this gap.

This upper bound can be obtained by considering an ideal offset assignment, which minimizes the worst-case ETE delay for all the flows. This ideal assignment may not exist for a given configuration, but it is sure that it gives worst-case delays which are not higher than the ones obtained by the *optimal offset assignment*. This ideal assignment, denoted *IdealAssign*, minimizes the maximum waiting delay of every frame in each output port it crosses. It corresponds to the following scenario:

- At its source ES, a frame f_i of a VL v_i is not delayed by any other frames emitted by the same ES, i.e., the frame f_i is transmitted immediately after its release;
- At each switch output port of its path, the frame f_i crosses VLs generated by several ESs. f_i can be delayed by exactly one frame coming from each of these ESs. The frame with the largest size S_{max} is considered. The delay encountered by f_i at each switch output port takes into account the serialization effect (i.e., two frames cannot be received at the same time from an input link, see [3] for details).

Indeed, since there is no common clock among the end systems, there is no relationship between the releases of two frames from different end systems. Consequently, there exist scenarios where the two frames arrive at their first common switch output port at the same time.

Let us illustrate this scenario on the example depicted in Figure 2. This sample network has 4 VLs v_1 and v_2 emitted by the ES e_1 as well as v_3 and v_4 emitted by the ES e_2. The network works at $100\ Mb/s$. The temporal characteristics of each VL are listed in Table III.

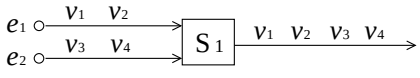

Figure 2. A sample AFDX network

v_i	BAG_i (ms)	S_{max_i} $(Byte)$	C_i (μs)
v_1	8	1000	80
v_2	8	1000	80
v_3	8	1000	80
v_4	8	500	40

Table III
The Configuration of the sample example in Figure 2

The VL v_1 is focused on. The *IdealAssign* leads to scenario illustrated in Figure 3 where the arrow represents the frame arrival of VL v_i, a_i^h is the frame arrival of v_i at the node h, and the $\boxed{\text{i}}$ means the transmission of a frame of VL v_i. At the ES e_1, the frame f_1 is transmitted as soon as it is released due to the separation from v_2. Since the ESs are not synchronized, at the output port of the switch S_1, the frame f_1 of v_1 can arrive at the same time as the frame f_3 of v_3 and it is delayed by f_3, i.e., $a_1^{S_1} = a_3^{S_1}$. Only one frame (f_3) from the ES e_2 delays the frame f_1 at the output port of S_1 since v_3 and v_4 are separated far away from each other, and f_3 is considered due to the frame size $S_{max_3} > S_{max_4}$.

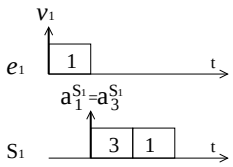

Figure 3. Scenarios of the VL v_1

The *IdealAssign* gives an upper bound on the reduction which can be obtained by an offset assignment algorithm. The next section proposes some offset assignment heuristics tailored for the AFDX network.

IV. Offset assignments in the context of AFDX network

In the context of a uniprocessor, a set of tasks shares a unique resource, i.e., the processor. The situation is different in the context of a switched Ethernet network, like the AFDX network, where a set of flows shares a set of output ports. Actually, each port is shared by a subset of all the flows. Consequently, the load can be different for each output port. The worst waiting time of a frame in an output port increases when the load of the output port increases. Then, it could be interesting to take into account the load of the output port in the offset assignment. This is illustrated in the example in Figure 4, where six VLs v_i ($i \in [1, 6]$) are transmitted over the network. The temporal characteristics of each VL are given in Table IV. The network works at $100\ Mb/s$ and the technological latency of switch is null.

The offset assignment *SingleAssign* is applied to this example network. The three VLs emitted by the ES e_1 are considered. The offsets are assigned to these three VLs in

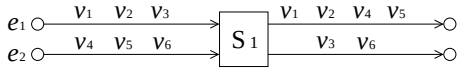

Figure 4. A small example of AFDX network

v_i	BAG_i (μs)	S_{max_i} ($Byte$)	C_i (μs)
v_1	400	500	40
v_2	800	750	60
v_3	400	750	60
v_4	400	500	40
v_5	800	750	60
v_6	400	750	60

Table IV
THE CONFIGURATION OF THE SMALL EXAMPLE IN FIGURE 4

order: $O_1 = 0\ \mu s$, $O_3 = 200\ \mu s$ and $O_2 = 100\ \mu s$. This case is drawn in part e_1 in Figure 5. Similar case at the end system e_2 is depicted in part e_2 in Figure 5. v_2 is focused on whose first frame f_2 is released at $O_2 = 100\ \mu s$. At the output port of the switch S_1 where v_2 visits, v_4 and v_5 from e_2 join the path of v_2 while v_3 has left. Then one possible scenario at this output port is depicted in part S_1 in Figure 5. It can be seen that when the frames f_1 and f_2 arrive at S_1, they are still separated far enough to avoid delaying each other. Similarly, the frames f_4 and f_5 from v_4 and v_5 are separated far enough when they arrive at S_1, consequently only one frame f_5 delays the studied frame f_2. Since the frame f_2 is released at the ES e_1 at time $O_2 = 100\ \mu s$ and the transmission of frame f_2 is finished at the switch S_1 at time $280\ \mu s$, the delay of the frame f_2 is $R_2 = 280 - 100 = 180\ \mu s$.

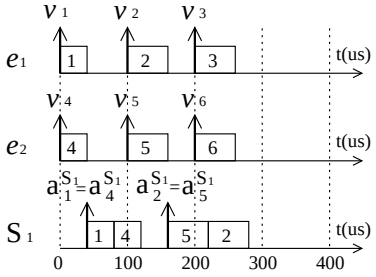

Figure 5. Illustration of the *SingleAssign* with low workload

The illustration in Figure 5 shows an example where the offset assignment *SingleAssign* succeeds to distribute the workload even in the output port of a switch. It is interesting to demonstrate the case when the workload increases. The example AFDX network in Figure 4 is under study and the maximum frame sizes of VLs v_1 and v_4 are increased to $S_{max_1} = S_{max_4} = 750\ Bytes$ ($C_1 = C_4 = 60\ \mu s$). According to the *SingleAssign*, the releases of frames at e_1 and e_2 are depicted in Figure 6 (same as in Figure 5). One possible scenario at the output port of S_1 is exhibited in part S_1 in Figure 6, where the studied frame f_2 finishes its transmission at time $300\ \mu s$. The delay of the frame f_2 is $R_2 = 300 - 100 = 200\ \mu s$, higher than the case in Figure 5 ($180\ \mu s$). It increases due to the fact that when the frame f_2 arrives at S_1 at time $a_2^{S_1} = 160\ \mu s$, the transmission of frame f_4, delayed by the transmission of frame f_1, is not completed which delays the transmission of frame f_2. For this case the *SingleAssign* could not separate frames at a crossed switch.

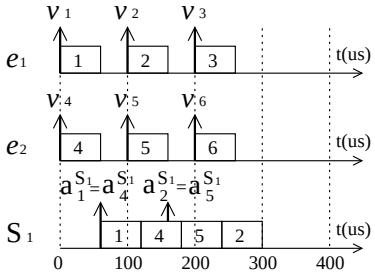

Figure 6. Illustration of the *SingleAssign* with high workload

Note that v_1, v_2 and v_3 emitted by e_1 visit three output ports: e_1 with the utilization $U_{e_1} = \sum(\frac{C_1}{T_1} + \frac{C_2}{T_2} + \frac{C_3}{T_3}) = 0.375$; the upper output port of S_1 with the utilization $U_{S_1} = \sum(\frac{C_1}{T_1} + \frac{C_2}{T_2} + \frac{C_4}{T_4} + \frac{C_5}{T_5}) = 0.45$; and the lower output port of S_1 with the utilization $U_{S_1'} = \sum(\frac{C_3}{T_3} + \frac{C_6}{T_6}) = 0.3$. Consequently, for these three VLs, the most loaded port is the upper output port of S_1, followed by e_1 and the lower output port of S_1. We could first assign offsets to v_1 and v_2 which visit the most loaded port of S_1, then pass to the v_3, leading to the offsets: $O_1 = 0\ \mu s$, $O_2 = 200\ \mu s$ and $O_3 = 100\ \mu s$. This case is illustrated in part e_1 in Figure 7. Similar case for the VLs emitted by e_2 is shown in part e_2 in Figure 7. Then one possible scenario for the frame f_2 at S_1 is identified in part S_1 in Figure 7, indicating that the delay of this frame is $R_2 = 380 - 200 = 180\ \mu s$, which is smaller than the one obtained by *SingleAssign* ($200\ \mu s$). The reason is that at the most loaded output port of S_1 the workload is further evenly distributed to reduce the waiting time in the buffer.

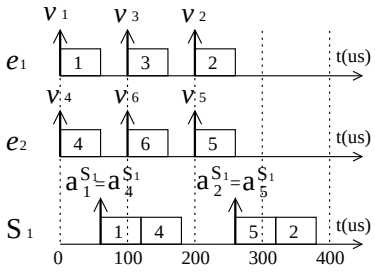

Figure 7. Illustration of the *MostLoadSA* with high workload

A proposed algorithm considers separating the VLs by

decreasing utilization of the output ports they share. The offsets are first assigned to the flows visiting the most loaded port using the assignment *SingleAssign*, then to the flows which are not yet handled in the secondly most loaded port till all the flows of one ES are assigned with offsets. This algorithm is developed based on the assignment *SingleAssign* and denoted *MostLoadSA*.

For the *PairAssign*, a similar heuristic is proposed to consider the load of the output ports. This heuristic, denoted $MostLoad$, sorts the VL pairs (v_i, v_j) by decreasing values of $Ld_i + Ld_j$, where Ld_i is the workload (utilization) of most loaded switch port crossed by v_i.

Due to the nature of the switched Ethernet, flows in one set can share several output ports. When flows share several common switches, the minimum interval between two frames decreases, which can increase the waiting time of a frame in the output port. Then the number of crossed switches can be considered in the offset assignments. For the *PairAssign*, a heuristic, denoted $CrossedS$, is proposed. It sorts the VL pairs (v_i, v_j) by decreasing values of $cs(v_i, v_j)$, where $cs(v_i, v_j)$ is the number of common switches crossed by v_i and v_j. For the *SingleAssign*, a similar heuristic, denoted *CrossedSSA*, is proposed which orders the VLs in one set by decreasing values of maximum number of crossed switch.

Besides the four new proposed heuristics, the existing offset assignment heuristics presented in Section II-B are applied to the AFDX network with the value of BAG as the period. The evaluation on each offset assignment is processed in the next section.

V. Obtained results

The existing and proposed offset assignments introduced in Section IV are applied to the industrial AFDX network presented in Section II-A. In this evaluation, all the VLs are assumed to be strictly periodic. The computation is processed using the Network Calculus approach integrating the offsets, which has been developed in [7]. The computed ETE delay upper bounds of each offset assignment are compared with those obtained from the network without offset constraints. The statistic reductions on ETE delay upper bounds of each algorithm are listed in Table V. The columns *Average*, *Max* and *Min* give the average, maximum and minimum reductions, respectively.

The *SingleAssign* as well as its extended algorithms *MostLoadSA* and *CrossedSSA* outperform the *PairAssign* heuristics. Indeed, the average reductions obtained with the *PairAssign* heuristics are 23% (*GCD*) and 32% (*RateAdd*, *RAGCD*, *RMGCD*, *GCDMinus*, *MostLoad* and *CrossedS*). It is 49% for the *SingleAssign* and 51% for the *SingleAssign* based algorithms adapted to the AFDX network. On the considered example, the *SingleAssign* based algorithms are close to the *IdealAssign*, which gives an average reduction of 53%.

Heuristics	Average %	Max %	Min %
IdealAssign	53.48	83.29	21.00
GCD	23.00	70.24	4.01
RateAdd	32.89	73.50	5.08
RAGCD	32.51	72.99	8.85
RMGCD	32.29	70.77	9.99
GCDMinus	32.95	70.06	8.83
MostLoad	32.12	70.06	8.84
CrossedS	32.32	73.03	8.90
SingleAssign	49.67	83.29	18.84
MostLoadSA	51.32	82.94	18.84
CrossedSSA	51.29	82.94	18.84

Table V
THE COMPARATIVE RESULTS

The *PairAssign* heuristics are not efficient in the studied context due to the limited different values of BAG, which lead to same values of $gcd(BAG_i, BAG_j)$ for different VL pairs. Here is a small example in Figure 8. Considering VLs v_1, v_2 and v_3 with $BAG_i = 4\ ms$ ($i \in [1, 3]$) of e_1, there are three pairs: (v_1, v_2), (v_1, v_3) and (v_2, v_3). They have the same value of $gcd(BAG_i, BAG_j) = 4\ ms$ ($1 \leq i < j \leq 3$). *GCD* leads to $O_1 = 0\ ms$, $O_2 = O_1 + \frac{gcd(BAG_1, BAG_2)}{2} = 2\ ms$, and $O_3 = O_1 + \frac{gcd(BAG_1, BAG_3)}{2} = 2\ ms$ ($O_2 = O_3$). The releases of the first frames for both v_2 and v_3 overlap, and the frames have to wait in the queue. This case is depicted in Figure 9.

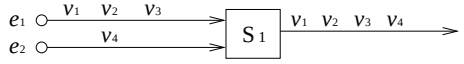

Figure 8. A small example of AFDX

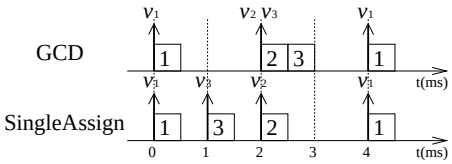

Figure 9. Comparison of GCD and SingleAssign

The situation is different when applying the offset assignment *SingleAssign* (Figure 9). With the same configuration, the offsets are set in order: $O_1 = 0\ ms$, $O_2 = 2\ ms$ and $O_3 = 1\ ms$. In this way, no frame has to wait in the output queue of e_1.

The analyzed problem of *GCD* for the industrial AFDX network exists for all the *PairAssign* heuristics because the computation of offsets mainly concerns the value of $gcd(BAG_i, BAG_j)$ even if the order of pairs varies based on different criteria.

The results are further studied by a normalized method. For one path $\mathcal{P}_x$, the computed ETE delay upper bound without offset assignment is considered as the reference

(denoted rf_x) and normalized as 100. The computed result with one offset assignment (denoted cp_x) is taken as the comparison and normalized as Ncp_x:

$$Ncp_x = 100 + (\frac{cp_x - rf_x}{rf_x} \times 100)$$

All the 6412 VL paths are sorted by increasing order of Ncp_x. Three offset assignments are taken into account: *IdealAssign*, *SingleAssign*, and *MostLoadSA*. The comparative results are presented in Figure 10.

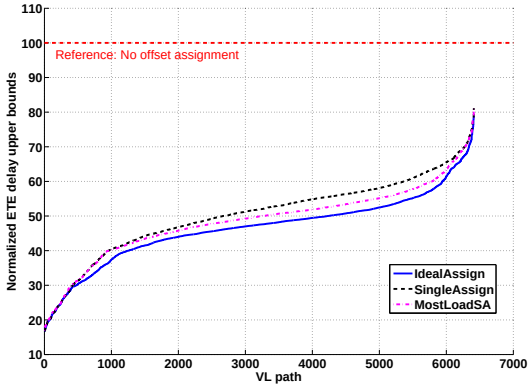

Figure 10. Comparative results of *IdealAssign*, *SingleAssign* and *MostLoadSA*

It can be seen in Figure 10 that the *MostLoadSA* curve is close to the *IdealAssign* curve, which reveals that this algorithm taking into account the AFDX properties works well on this industrial AFDX network. The gap between the *SingleAssign* curve and the *IdealAssign* curve is also small (although bigger than the gap with *MostLoadSA* curve). It suggests that a simple algorithm could be efficient to separate the flows of the industrial AFDX network.

Further evaluations have been conducted, leading to the same conclusions. They consider the same industrial AFDX architecture described in Section II-A and the overall workload 10% is kept. For each VL, the S_{min} and S_{max} are randomly chosen from 72 $bytes$ to 1526 $bytes$, and the BAG value is randomly chosen from 1 ms to 128 ms as the powers of 2. The results show that the average ETE delay reduction brought by the $IdealAssign$ is 45%. The $PairAssign$ heuristics bring average reductions ranging from 24% to 31%, which are far from the $IdealAssign$. The algorithms based on the $SingleAssign$ bring average reductions ranging from 39% to 40%, which are closer to the $IdealAssign$.

VI. Conclusion

In this paper, the offset assignments for the industrial AFDX network are studied. Since the *optimal offset assignment* is intractable in this context, an optimal scenario is built based on a presumed ideal assignment in order to upper bound the gap between the *optimal offset assignment* and each offset assignment heuristic. New heuristics considering the AFDX characteristics are proposed. Using the Network Calculus approach, the improvement on ETE delay upper bound bought by each heuristic is compared to the ideal algorithm. It is demonstrated that *PairAssign* heuristics are not efficient when applied to the industrial AFDX network due to the limited different values of BAG. The *SingleAssign* turns out a near optimal algorithm in the studied context. Although the heuristics integrating specific AFDX characteristics bring slight improvements in contrast to the *SingleAssign*, they are of increased complexity.

The industrial AFDX network considered in this paper is lightly loaded. The offset assignment for a switched Ethernet with heavier workload remains an open question, which is the subject of our ongoing work.

References

[1] *ARINC 664*, ACCE Std. 664, 2002-2008.

[2] F. Frances, C. Fraboul, and J. Grieu, "Using network calculus to optimize the AFDX network," in *Proc. 3rd Embedded Real Time Software Conference (ERTS'06)*, Toulouse, Jan. 2006.

[3] H. Bauer, J.-L. Scharbarg, and C. Fraboul, "Improving the worst-case delay analysis of an AFDX network using an optimized trajectory approach," *IEEE Trans. Ind. Informat.*, vol. 6, no. 4, pp. 521–533.

[4] J.-L. Scharbarg, F. Ridouard, and C. Fraboul, "A probabilistic analysis of end-to-end delays on an AFDX avionic network," *IEEE Trans. Ind. Informat.*, vol. 5, no. 1, pp. 38–49, Feb. 2009.

[5] H. Charara, J.-L. Scharbarg, J. Ermont, and C. Fraboul, "Method for bounding end-to-end delays on an AFDX network," in *Proc. the 18th Euromicro Conference on Real-Time Systems (ECRTS'06)*, Germany, Jul. 2006, pp. 192–202.

[6] J.-Y. L. Boudec and P. Thiran, *Network Calculus: A Theory of Deterministic Queuing Systems for the Internet*, ser. Lecture Notes in Computer Science. Springer-Verlag, 2001, vol. 2050, iSBN: 3-540-42184-X.

[7] X. Li, J.-L. Scharbarg, and C. Fraboul, "Improving end-to-end delay upper bounds on an AFDX network by integrating offsets in worst-case analysis," in *Proc. IEEE International Conference on Emerging Technologies and Factory Automation (ETFA'10)*, Bilbao, Spain, Sep. 2010, pp. 1–8.

[8] M. Grenier, L. Havet, and N. Navet, "Pushing the limits of CAN - scheduling frames with offsets provides a major performance boost," in *4th European Congress on Embedded Real Time Software*, Toulouse, France, Jan. 2008.

[9] J. Goossens, "Scheduling of offset free systems," *Real-Time Systems*, vol. 24, no. 2, pp. 239–258, Mar. 2003.

[10] M.Grenier, J. Goossens, and N. Navet, "Near-optimal fixed priority preemptive scheduling of offset free systems," in *Proc. 14th International Conference on Real Time Network and Systems (RTNS'06)*, Poitiers, France, May 2006.